WIDE ANGLE AVO/AVAZ INVERSION

JOSHUA C. LELAND

MSC INTEGRATED PETROLEUM GEOSCIENCES

2014 - 2015

DEPARTMENT OF EARTH AND ATMOSPHERIC SCIENCE

DEPARTMENT OF PHYSICS

UNIVERSITY OF ALBERTA

SUPERVISOR: PROFESSOR MAURICIO SACCHI

Declaration

I Joshua C. Leland confirm that this report and the work it describes is my own and the report is written in my own words. Any use made within the report to the works of other authors in any form (e.g., ideas, equations, figures, text, tables, programs) are given proper acknowledgement at the point of their use. A list of references is also included.

Signed:

Date: July 31, 2015

Contents

List of Figures

1 Acknowledgements

I would like to thank my supervisor Dr. Mauricio Sacchi for the excellent guidance he has provided over the course of this project. I would also like to thank the members of the Signal Anaysis and Imaging group for being enthusiastic with help, questions, or concerns that I had. Most importantly, I would like to thank my Father for his endless support and love. This would all not be possible without him.

2 Abstract

AVO/AVAz (amplitude variation with offset/amplitude variation with azimuth) looks at changes in reflectivity of an interface in the subsurface with respect to offset and azimuth. The variation with offset is used to infer material properties in the ground. Inversion of AVO/AVAz attempts to find a subsurface model that can reproduce the data found in the field, and that is also as close as possible to what is known about the area a priori.

This paper uses a method that can be applied to both AVO and AVAz inversion and can overcome both the ill conditioned and ambiguous nature of the problem by using the well log data. To solve the problem a cost function is developed that will minimize the misfit between predicted and observed data only to the noise level, while constraining the data to be close to the general trends derived from the well log data, and have the covariance between the material parameters be close to the parameters in the well logs.

Synthetic data were generated to test the sensitivity of the method to different errors in the forward model and found it was most sensitive to the wavelet and incorrect angles of incidence. It displays the importance of making sure the wells are tied with a carefully chosen wavelet, as well as using the most accurate method possible to estimate the angle of incidence.

Real data from Puesto Peter Field, Argentina, was then inverted using the method. The area was a good candidate for the method with good well control that was representative of the geology in the 2D line that is being inverted. When the data was inverted it was compared to the known geology from the basin and found to be accurate. A successful inversion using this method showed simple, fast method with smart regularization can give very realistic and interpretable results. Caution must be taken to make sure the assumptions made are valid or else costly mistakes can be made. Inversion does not add anything to the data, but is just the reformation of a collection of data, and because of this inversion is always limited to the validity of its assumptions and data quality.

3 Introduction

3.1 Introduction to Inversion and AVO

Forward modelling is the process to obtain simulated data a model via governing equations or principles. Examples of this from geoscience are: predicting tectonic movements, predicting gravity or magnetic anomalies, predicting seismic responses, and using geological information to predict reservoir qualities. Inverse modelling is then taking a set of data and predicting parameters of the governing equations or principles that describe the behaviour. Inverse modelling in geoscience has examples of: predicting density anomalies in the ground from gravity, imaging the conductive structure in the ground from injecting current into the ground, and predicting elastic properties in the ground from seismic data. Most of these inverse problems suffer from ambiguity and being ill conditioned, and as a result it is critical to integrate a priori knowledge to constrain the inverse problem in order to get a solution that is reasonable.

Reflection seismology measures the energy reflected to the surface from an interface in the subsurface. Most commonly, this is used to image interfaces of changes in material properties in the subsurface to uncover the structural geology. The strength of reflection sent back to the surface (commonly called reflectivity) is a function of the change in material properties at an interface and the angle of incidence of the incoming wave. The non-linear equations governing the reflectivity and transmissivity for pressure and shear waves are called the Zoeppritz equations (Chopra and Castagna, 2014). AVO is very often analyzed using a slope gradient method shown in Gidlow and Smith (2003), but this paper will focus on AVO/AVAz inversion.

AVO/AVAz inversion uses seismic data that has been processed but pre-stacked, and takes a prior information about the area such as geological information from well logs to generate a likely earth model that will produce the same AVO response (Chopra and Castagna, 2014). This likely earth model is very useful for interpretation of the material properties an area, which can give a lot on insight into the economic potential. AVO inversion is often referred to as pre-stack inversion because it uses the data before it is stacked, as opposed to post-stack inversion which inverts the data after it is stacked (Yilmaz, 1990).

Post stack inversion will solve for the P wave impedance, while in this paper we will be solving for the P wave velocity, S wave velocity and density (Chopra and Castagna, 2014).

This paper will examine theory, methods, and results of prestack inversion. It will investigate popular methods for prestack inversion used in industry. Popular industry methods generally use a small incidence angle approximation for their forward model. While this approximation helps with stability, it limits the use of data to angles of incidence to less than 30 degrees (Chopra and Castagna, 2014; Goodway et al., 2006a). Using ideas from papers like Buland and Omre (2003) and Theune et al. (2010) we will use an efficient stable method that will allow us to use a more accurate forward model that can use incidence angles less than the critical angle (Chopra and Castagna, 2014).

The paper will then extend the method from the isotropic case to the case of anisotropic media. Media with vertical fractures is common in carbonates and unconventional shales and being able to understand what impact the vertical fractures has on the reflectivity will help characterize the reservoir for important features like increased permeability or brittleness (Goodway et al., 2006b; Chen et al., 2014; Roxana Varga and Pendrel, 2013). By using the more mature methods and ideas from the isotropic case, this paper will look at making a general formulation that can be applied to the less mature anisotropic case. Results from the synthetic data will help outline the strengths and weaknesses of the general formulation. An inversion will then be done on a real data set from Puesto Peter Field, Austral Basin, Argentina to demonstrate the ability of the method to handle real data and will be followed by some interpretation of the results. By the end of this paper three fundamental questions will be answered: what is AVO/AVAz inversion? How does it work? And most importantly why do inversion?

4 Theory

This section will talk about the theoretical reasons and implications behind the common choices of the approximations for forward modelling and inversion. Having a solid basis in understanding the approximations are essential. If the approximations are not well understood then it can easily be miss applied and significant error is introduced. When dealing

with economic resources having more error means having more risk, and when risk is not properly assessed costly mistakes are made. Forward modelling and inverse modelling both have their own set of assumptions that must be understood for accurate solutions. In the forward modelling section we will look at various forward models, their assumptions, and their pitfalls. In the inverse section we will look at popular techniques for regularization, and ambiguities that are common to the AVO/AVAz inverse problem and how to overcome them.

4.1 Forward modeling

A compressional plane wave incident to a subsurface interface will have its energy split into compressional and shear waves. The fractional energy make up of each of the transmitted and reflected P and S waves are completely described by the Zoeppritz equations. Nafe (1957) was able to express the equation as a matrix in equation (1) for a wave traveling from a medium 1 to a medium 2 with the following expression in equation (1). The expression is illustrated in figure 1.

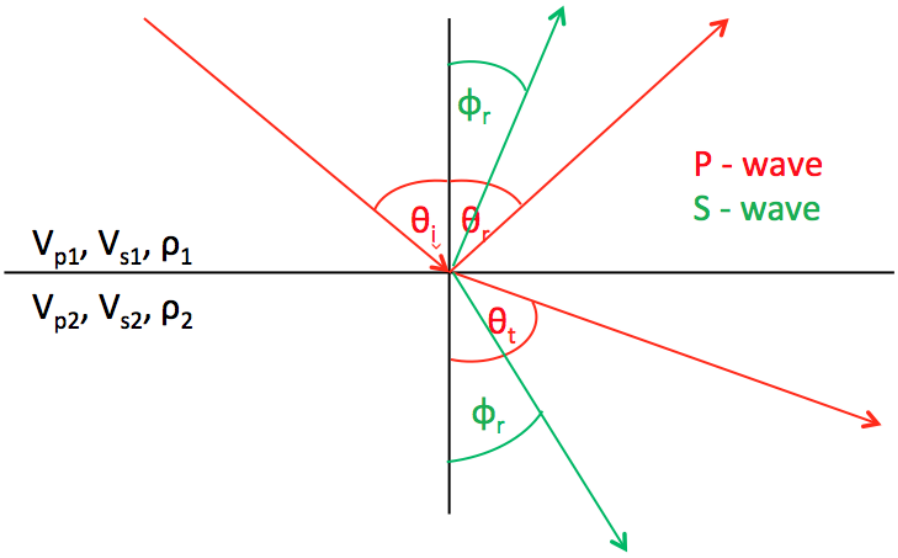

Figure 1: Graphic showing the interaction of a incident P wave on a interface.

$$\begin{bmatrix} cos\theta_i & \frac{V_{P_1}}{V_{S_1}}sin\phi_r & \frac{V_{P_1}}{V_{P_2}}cos\theta_t & -\frac{V_{P_1}}{V_{S_1}}sin\phi_r \\ -sin\theta_i & \frac{V_{P_1}}{V_{S_1}}cos\phi_r & \frac{V_{P_1}}{V_{P_2}}sin\theta_t & \frac{V_{P_1}}{V_{S_1}}cos\phi_t \\ -cos2\phi_r & -sin2\phi_r & \frac{\rho_2}{\rho_1}cos2\phi_t & \frac{-\rho_2}{\rho_1}sin2\phi_t \\ sin2\theta_i & -\frac{V_{P_1}^2}{V_{S_1}^2}cos2\phi_r & \frac{\rho_2}{\rho_1}\frac{V_{S_2}^2}{V_{S_1}^2}\frac{V_{P_2}^2}{V_{P_1}^2}sin2\theta_t & \frac{\rho_2}{\rho_1}\frac{V_{P_1}^2}{V_{S_1}^2}cos2\phi_t \end{bmatrix} \times \begin{bmatrix} R_{pp} \\ R_{ps} \\ T_{pp} \\ T_{ps} \end{bmatrix} = \begin{bmatrix} cos\theta_i \\ sin\theta_i \\ cos2\phi_r \\ sin2\theta_r \end{bmatrix} \quad (1)$$

where

- θ_i is the angle of incidence with respect to the normal of the interface.
- θ_t is the angle of transmission of the P wave with respect to the normal of the interface.
- ϕ_t is the angle of transmission of the S wave with respect to the normal of the interface.
- ϕ_r is the angle of reflection of the S wave with respect to the normal of the interface.
- V_{P_i} is the P wave velocity of the *i*th medium.
- V_{S_i} is the S wave velocity of the *i*th medium.
- ρ_i is the density of the *i*th medium.
- R_{PP} is the energy reflected as a P wave.
- R_{PS} is the energy reflected as a S wave.
- T_{PP} is the energy transmitted as a P wave.
- T_{PS} is the energy transmitted as a S wave.

Equation (1) can be used to solve for the reflectivity and transmissivity for both the P and S waves if the velocities, densities and angles are known. The matrix is non linear with respect to the angles and inverting this forward model for velocities would require non-linear inversion methods. These non-linear methods are much more complicated to solve

and have a high computational cost. By making a few key assumptions Aki and Richards (1980) were able to linearize equation (1) for PP interfaces. The equation assumes the change of the elastic parameters is small from one interface to the other and that the angle of incidence is less than the critical angle (Chopra and Castagna, 2014)

$$R_{PP}(\theta) = \frac{1}{2}[1 + tan^2\theta]\frac{\Delta V_P}{\bar{V_P}} - \left[4\frac{\bar{V_S}^2}{\bar{V_P}^2}sin^2\theta\right]\frac{\Delta V_S}{\bar{V_S}} + \frac{1}{2}\left[1 - 4\frac{\bar{V_S}^2}{\bar{V_P}^2}sin^2\theta\right]\frac{\Delta\rho}{\bar{\rho}} \quad (2)$$

where

- $\bar{V_P}$ is the average P wave velocity.
- $\bar{V_S}$ is the average S wave velocity.
- θ is the average angle of incidence between the two layers.

Equation (2) is linear with respect to the model perturbations. The change in material properties is linearly proportional to the amount of energy that is reflected back to the surface for a P wave. This equation also makes it easier to see one of the pitfalls with seismic: the amount of energy sent back to the surface requires a significant, abrupt change in material properties. If the change in material properties is very small then R_{PP} is going to be close to zero and no energy will be reflected back to the surface to be recorded. This equation will be the main forward model for this paper but in industry it is common to use two term approximations to make inversion more stable (Alemie and Sacchi, 2011; Goodway et al., 2006b; Chopra and Castagna, 2014). A few examples of a two term approximations are below:

$$R_{PP}(\theta) = \left(\frac{5}{8} + \frac{1}{2}tan^2(\theta) - \frac{1}{2}\frac{\bar{V_S}^2}{\bar{V_P^2}}sin^2(\theta)\right)\frac{\Delta V_P}{\bar{V_P}} - 4\frac{\bar{V_S}^2}{\bar{V_P}^2}sin^2(\theta)\frac{\Delta V_S}{\bar{V_S}} \quad (3)$$

The equation (3) is called the Smith Gidlow approximation from Smith and Gidlow (1987) and uses Gardner's relation of $\rho = aV_p^{\frac{1}{4}}$ to simplify the density term. By using this approximation you are going to have error any time the true earth model deviates from

Gardner's relation. See Gardner et al. (1974) for more information on Gardner's relation. Equation (4) uses the approximation of small angles and assumes nothing about density and is referred to at the Fatti two term approximation (Chopra and Castagna, 2014).

$$R_{PP} = \frac{1}{2}\left(1 + tan^2(\theta)\right)\frac{\Delta I_P}{\bar{I_P}} - 4\left(\frac{\bar{V_S}^2}{\bar{V_P}^2}\right) sin^2(\theta)\frac{\Delta I_S}{\bar{I_S}} \tag{4}$$

Where:

- I_P and $\bar{I_P}$ are the P wave impedance and average P wave impedance respectively.
- I_S and $\bar{I_S}$ are the S wave impedance and average S wave impedance respectively.

In order to stabilize the equation, there are assumptions need to be made about the model. Equation (3) assumes the behaviour of the density in the model. In equation (4) the model assumes small incidence angles. The importance in understanding the assumptions in the models becomes very clear. If we wanted to do a two term inversion and our density was well behaved we can use equation (3) because we can use all of the field data, but if the density is quite anomalous we would need to use equation (4) because the departure of density from Gardner's relation would make our assumptions incorrect and introduce error into our inversion. Later on we will look at a method for constraining the material properties to allow for stable inversion of (2) with out having to cut our forward model down to two terms.

We have looked at forward modelling reflectivity in the ground for an isotropic medium, and now it is time to look forward models for anisotropic media. There are two areas of anisotropy that are commonly mentioned: horizontal fractured media and vertical fractured media (Goodway et al., 2006a; Close et al., 2010). Horizontally fractured media is generally modelled as bedded shales. Vertically fractured media is found in carbonate environments as karst, or in brittle shales that have been deformed. Goodway et al. (2006b) shows there is a ambiguity between horizontally fractured media and vertically fractured media, and Goodway et al. (2006b) states the effects on reflectivity are much larger for vertically fractured media than horizontally fractured media. The focus of this paper will be on vertical fractured media as it is much more important in reservoir analysis and its

effects are higher magnitude. The linearized equation that describes the reflection coefficient with respect to incidence, azimuth, velocity, density, and the Thomsen parameters are shown in Rüger (1997) and it was rewritten by Mahmoudian et al. (2012) in a form similar to equation (2). The linearize equation for vertically fractured media is shown below in equation (5) and a graphic illustrating the geometry for AVAz problem with vertically fractured media is shown in figure 2. The figure is in plane view with the vertical fractures in green.

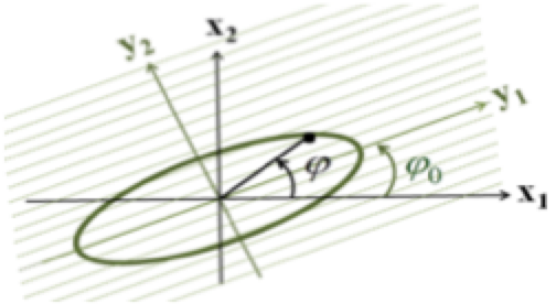

Figure 2: Figure illustrating the geometry for the vertically fractured AVAz problem. Figure from Mahmoudian et al. (2012)

$$R_{PP}(\theta,\phi) = A(\theta)\frac{\Delta V_P}{\bar{V_P}} + B(\theta)\frac{\Delta V_S}{\bar{V_S}} + C(\theta)\frac{\Delta \rho}{\bar{\rho}} + D(\theta,\phi)\Delta\delta + E(\theta,\phi)\Delta\epsilon + F(\theta,\phi)\Delta\gamma \tag{5}$$

where

- ϕ is the azimuth with respect to the fracture strike. ϕ is represented by $\varphi - \varphi_0$ in figure 2.
- $A(\theta), B(\theta), C(\theta)$ are the same coefficients as in equation (2).
- $D(\theta,\phi) = \frac{1}{2}\left(cos^2\phi sin^2\theta + cos^2\phi sin^2\phi sin^2\theta tan^2\theta\right)$
- $E(\theta,\phi) = \frac{1}{2}cos^4\phi sin^2\theta tan^2\theta$
- $F(\theta,\phi) = \frac{4\bar{V_S}^2}{\bar{V_P}^2}cos^2\phi sin^2\theta$
- δ is the wave splitting parameter.

- ϵ is the fractional difference in the P wave velocity of the vertical and horizontal directions.

- γ is the fractional difference in the S wave velocity of the vertical and horizontal directions.

Equation (5) is a very complex but very powerful equation. It should be remembered that this assumes anisotropy due to only vertical fractures. Similar to the isotropic case there are inversion schemes that will make assumptions to bring this six term equation down to a four term equation to facilitate smoother inversions. An example of this can be found in Chen et al. (2014). For this paper we will focus on using the full six term Rüger equation for inversion.

4.2 Inversion

In the previous section we discussed the forward models that are used in this paper. In this section we will discuss the solutions for inverting the data into model space. As talked about in the introduction the problem is ill-conditioned and will need a priori knowledge to find a reasonable, stable solution. For most geoscience inversion problems there are two goals: find a model that fits the data, and find a model that is close to our a priori knowledge. We want a model that will fit the data to the noise level, and that is close to what we know from geological knowledge such as: well logs, stratigraphy, etc. If the data is fit too closely there will be features in the model that are a product of the noise and not the data. To describe this equation mathematically a cost function is developed and is shown in equation (6).

$$J = ||\mathbf{d_{obs}} - \mathbf{d_{pred}}||_2^2 + \mu||\mathbf{W_m}\left(\mathbf{m} - \mathbf{m_0}\right)|\,|_2^2 \tag{6}$$

- $\mathbf{d_{obs}}$ is the observed data.

- $\mathbf{d_{pred}}$ is the data predicted by the forward model.

- μ the trade off parameter.

- $\mathbf{m}$ is the model parameters.
- $\mathbf{m_0}$ are an a priori estimate of the model parameters.
- $\mathbf{W_m}$ is a weight matrix containing a priori knowledge about the model parameters.

The above equation illustrates the general inversion problem. The specifics about it will be discussed in the methods section. If we assume the forward model to be linear, which it is with equation (2) or equation (5), we can define $\mathbf{d_{pred}} = \mathbf{Gm}$ where $\mathbf{G}$ is the forward operator. Using the same formulation as Buland and Omre (2003) we can define $\mathbf{m} = [ln(V_P(t)), ln(V_S(t)), ln(\rho(t)))]^T$ for the isotropic case or $\mathbf{m} = [ln(V_P(t)), ln(V_S(t)), ln(\rho(t))), \delta(t), \epsilon(t), \gamma(t)]^T$ for the anisotropic case discussed above. The forward model is then defined as $\mathbf{G} = \mathbf{WRD}$ where $\mathbf{W}$ is the matrix convolution operator for the wavelet, $\mathbf{R}$ is the reflectivity operator like equation (2) or (5), and $\mathbf{D}$ is a discrete derivative operator. The forward operator is then the product of three operatons: taking the derivative of the parameters, computing the reflectivity, and convoluting with the wavelet to make the reflectivity a trace. The solution to equation (6) is shown below:

$$\mathbf{m} = \mathbf{m_0} + \left(\mathbf{G^T G} + \mu \mathbf{W_m^T W_m}\right)^{-1} (\mathbf{d_{obs}} - \mathbf{G m_0}) \tag{7}$$

Equation (7) can is derived by taking the derivative of equation (6) with respect to $\mathbf{m}$ and setting it to zero in order to find the minimum. The solution to this general inverse problem is also found in Menke (2012). It is possible to construct the matricies and solve this equation for this closed form solution, but this is never done in practice. The size of the matrices are too large for practical purposes to be solved this way. This paper will use a iterative methods to find the solution which will be discussed in the next section.

This section introduced the theory behind modelling AVO/AVAz and general inversion strategy for inverse problems. The next section will look at the practical methods applied to the theory to generate reasonable solutions and overcome the shortcomings and ambiguities associated with the AVO/AVAz problems.

5 Methods

5.1 Ambigutiy of the AVO/AVAz inverse problem.

As previously talked about in the theory section equations (2) and (5) are only sensitive to the derivative of the material properties when generating reflectivity. This acts as a high pass filter ignoring the slowly changing or constant material content in the ground. To demonstrate this figure 3 is shown below representing a 1D earth model in blue. In red is a smooth earth model with very small derivatives.

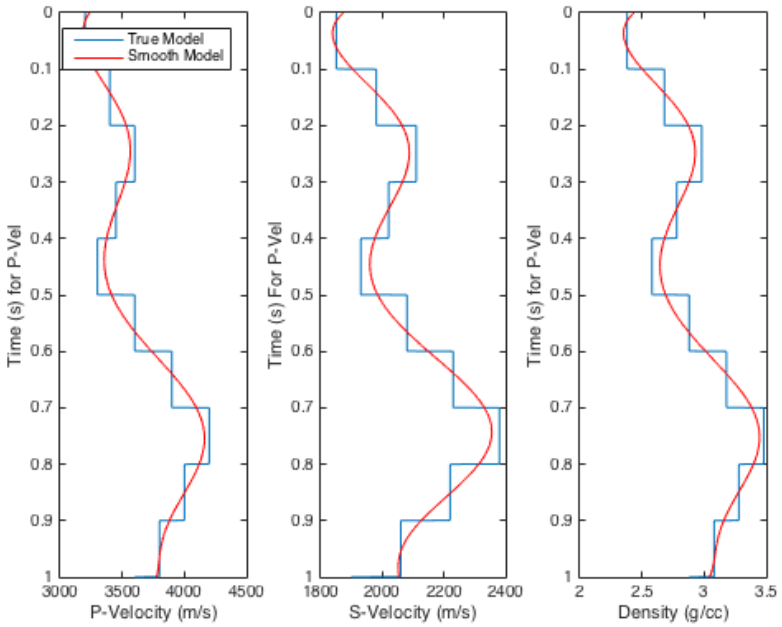

Figure 3: 1D earth model in blue, smooth background model in red.

By looking at the smooth part we can decompose the model into two parts: a smooth part, and a rough part. If we look at the AVO response for the True model and the smooth model we can see how much of the seismic response is contributed from the smooth part of the model. The responses are shown below:

Figure 4 shows a CMP gather for the two models. A CMP gather stands for common midpoint gather. All of the traces in figure 4 are looking at the same point in the earth, but with different distances between the source and receiver. If the edging effects from the modelling are ignored it is quite obvious that that any background response from the

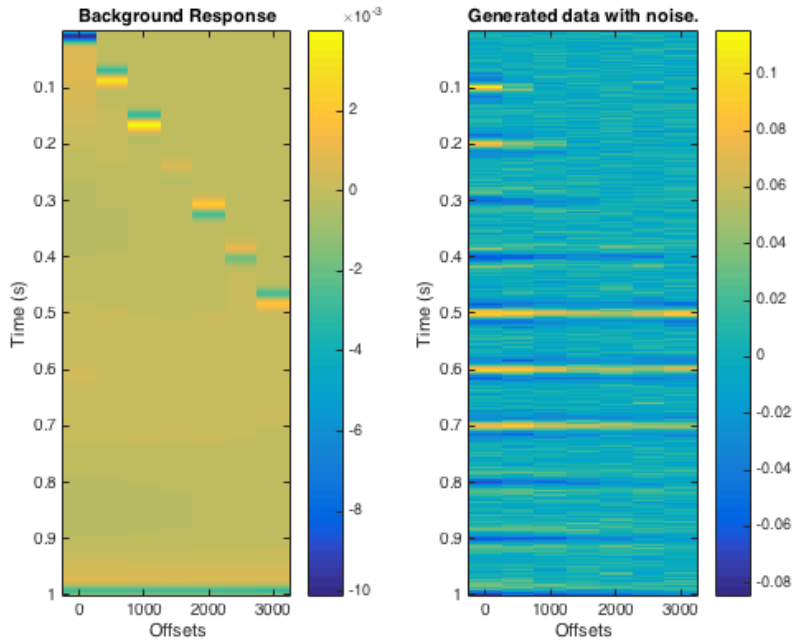

Figure 4: Seismic response of the smooth model and true model respectivly.

smooth model is not contributing any seismic significant response. This example now introduces the ambiguity problem in AVO/AVAz. If one was to take out the smooth model in figure 3 and replace it with a different smooth background model we would generate the same response. Trying to invert this data set without any a priori knowledge of the slowly varying changes in the ground would give erroneous results, so having some idea about the smooth trends of the dataset are necessary to get an accurate solution. Buland and Omre (2003) takes the average of the parameters from well log data, in this paper we pick a smooth background model from the well logs that will generate almost no seismic response and use that for the background model. This smooth background model is represented by $\mathbf{m_0}$ in equations (6) and (7).

5.2 The ill-conditioned nature of the AVO/AVAz inverse problem

The AVO/AVAz inversion problem is ill-conditioned. Ill-conditioned is when a small perturbation in data results in a large change in model parameters (Alemie and Sacchi, 2011). Lines (1999) was able to show that the AVO response is not very sensitive to fractional

changes in density. This poses to be a problem because when inverting because there are a wide range of densities that can give a similar AVO response, and can cause unreasonable density solutions when inverting. A solution to this problem has been shown in equation (3), which uses Gardner's relation to replace the density term. The density is then assumed to follow Gardner's relation, and will give a more stable inversion. However if density does not follow Gardner's relation error can be introduced when inverting for the velocities. Density is an important parameter for reservoir characterization, as we will see in the real data inversion section. Another solution to this is follow (4) which solves for the P and S wave impedance for only small impedance angles with the trade off of throwing away data. The solution used in this paper is to borrow ideas from Buland and Omre (2003), Theune et al. (2010), and Alemie and Sacchi (2011) to use the well logs to help stabilize the inversion.

We already use well log data to find a smooth background model that the forward model is not sensitive to, but well logs also have more information to them as well. There are many empirical correlations for correlating V_P, V_S, and ρ, (see Chopra and Castagna (2014) for many of them), which gives a basis for using the correlations between the model parameters from the well logs to help stabilize the inversion. Up until this point we assumed, mathematically, that the model parameters are independent and this, geologically speaking, is not true. For example if we take the sonic log of lithologic region that has carbonate cement we would expect V_P, V_S, and ρ to all increase in the cemented region. If we enter a gas filled region then we would expect V_P and ρ to drop dramatically, and V_S to not drop as drastically (Chopra and Castagna, 2014). The information from this is valuable and this a priori knowledge can be implemented to stabilize the inversion. To implement this information into the inversion we define a covariance matrix for the previously mentioned $\mathbf{m}$ from equation (7) for the isotropic case (Theune et al., 2010),

$$\Sigma_0 = \begin{bmatrix} \tau^2_{V_P} & \nu_{V_P,V_S} & \nu_{V_P,\rho} \\ \nu_{V_P,V_S} & \tau^2_{V_S} & \nu_{V_S,\rho} \\ \tau_{V_P,\rho} & \nu^2_{V_S,\rho} & \tau^2_{\rho} \end{bmatrix}, \tag{8}$$

where

- τ^2 is the variance of the logarithm of the material property from the well log.
- ν is the covariance between the logarithm of the material property.

We can then define the parameter weight matrix from equation (7) to be:

$$\mathbf{W_m^T W_m} = \begin{bmatrix} \Sigma_{0_1} & 0 & 0 & \dots \\ 0 & \Sigma_{0_2} & 0 & \vdots \\ \vdots & \dots & \ddots & 0 \\ 0 & 0 & 0 & \Sigma_{0_n} \end{bmatrix}^{-1} = \begin{bmatrix} \Sigma_{0_1}^{-1} & 0 & 0 & \dots \\ 0 & \Sigma_{0_2}^{-1} & 0 & \vdots \\ \vdots & \dots & \ddots & 0 \\ 0 & 0 & 0 & \Sigma_{0_n}^{-1} \end{bmatrix} \tag{9}$$

Where:

- Σ_{0_i} is the covariance matrix for the ith point in the subsurface.

This block matrix in equation (9) most of the time will be calculated from the entire well log and then then same covariance matrix applies to the all of the points in the subsurface. We also want $\mathbf{W_m^T W_m}$ to equal the inverse of the matrix because we want to maximize the effect of the covariance, and that can be done by minimizing the inverse, since we have to minimizine in the cost function. If there is a large unconformity running through data that may drastically change the covariance it can easily be split up into different sections. To explicitly calculate $\mathbf{W_m}$ singular value decomposition is a very good tool to use, and will be explained in the practical implementation section. This is similar to what Downton et al. (2004) did with eigenvectors for when trying to solve for sparse perturbations.

This method as mentioned above is used in quite a few papers for the isotropic case, but I could not find any papers which extended this to equation (5). This is quite surprising because it is very simple, fast and robust implementation. Estimation from of the Thomsen parameters from well logs is possible as shown in Prioul et al. (2007) and Sil (2013). Constructing the covariance matrix is done the exact same as shown in equations (8) and (9). Having identified and addressed the major problems for the AVO/AVAz inversion problem the last thing that needs to be covered is the practical implementation of the methods.

5.3 Practical Implementation

This paper has looked over the theory and methods for the AVO/AVAz inversion problem. So far the solutions we have looked at are closed form, linear algebraic equations. It is possible to solve the problem by constructing the matrices in a programming language and working out an explicit solution but it's just not practical. The forward matrix is very sparse and it is very big. If we have N points in the sub-surface, M in the number of offsets, and Z is the number of azimuths. The matrix $\mathbf{G}$ would be $NMZ \times 3N$ which would make $\mathbf{G^T G}$ $3N \times 3N$ which also needs to be inverted. The problem is just to big to be solved this way and iterative methods need to be utilized to solve the problem. The paper uses a conjugate gradient least squares (CGLS) algorithm to minimize a cost function in the form of

$$J = ||\mathbf{Az} - \mathbf{d}'||_2^2 + \mu||\mathbf{z}||_2^2, \tag{10}$$

where

- $\mathbf{A}$ is a linear operator.
- $\mathbf{d}'$ is a data vector.
- $\mathbf{z}$ is a parameter vector.

See Scales (1987) for more information on CGLS. Equation (10) is written in a linear algebraic form, but no matrices are needed. The algorithm needs a linear operator $\mathbf{A}$, the adjoint operation $\mathbf{A^T}$, the data vector $\mathbf{d}'$, and an initial guess $\mathbf{z_0}$. The CGLS algorithm will iterate until a stopping criteria is met, and a approximate minimum to equation (10) is found. What is great about this is it can all be done on the fly. No matrices need to be computed and only the parameter and data vector are held in memory. In order to use this algorithm we need to get our cost function into the form of equation (10). We will start with a cost function similar to Theune et al. (2010)

$$J = ||\mathbf{Gm} - \mathbf{d}||_2^2 + \mu(\mathbf{m} - \mathbf{m_0})^T\mathbf{W_m^T W_m}(\mathbf{m} - \mathbf{m_0}). \tag{11}$$

We can used singular value decomposition to equate $\mathbf{W_m^T W_m} = \mathbf{V\Lambda V^T}$ Where $\mathbf{V}$ is

a symmetric matrix and $\mathbf{\Lambda}$ is a diagonal matrix. $\mathbf{W_m}$ can be defined as $\mathbf{W_m} = \sqrt{\Lambda}\mathbf{V^T}$. Equation (11) can then be written as

$$J = ||\mathbf{Gm} - \mathbf{d}||_2^2 + \mu||\mathbf{W_m}\left(\mathbf{m} - \mathbf{m_0}\right)||_2^2. \tag{12}$$

We can then use a change of variables and set $\mathbf{z} = \mathbf{W_m}\left(\mathbf{m} - \mathbf{m_0}\right)$ which we can also solve for $\mathbf{m} = \mathbf{W_m^{-1}z} + \mathbf{m_0}$ which will then put equation (12) in the form

$$J = ||\mathbf{G}\left(\mathbf{W_m^{-1}z} + \mathbf{m_0}\right) - \mathbf{d}||_2^2 + \mu||\mathbf{z}||_2^2. \tag{13}$$

Lastly by defining $\mathbf{d'} = (\mathbf{d} - \mathbf{Gm_0})$ and $\mathbf{A} = \mathbf{GW_m^{-1}}$ equation (13) becomes equation (10). To do this inversion we calculate $\mathbf{d'}$, define our series of operations the make up $\mathbf{A}$, find the required adjoint series of operations $\mathbf{A^T}$, solve for $\mathbf{z}$, and transform $\mathbf{z}$ back to $\mathbf{m}$. It should also be mentioned we never explicitly calculate the inverse for $\mathbf{W_m}$ but rather using SVD to decompose Σ_0^{-1} define the matrix as shown for $\mathbf{W_m}$, take the inverse, and multiply the inverse matrix by all of the parameters in the code individually as an operation. This is faster, saves memory and is equivalent to multiplying by $\mathbf{W_m^{-1}}$. In this paper we define $\mathbf{A}$ and $\mathbf{A^T}$ as $\mathbf{A} = \mathbf{WRDW_m^{-1}}$, and $\mathbf{A^T} = \left(\mathbf{W_m^{-1}}\right)^T\mathbf{D^T R^T W^T}$. With the operations defined in the theory sections. Finding the adjoint operator can be done by writing out the operation in matrix form, taking the transpose, and then writing code to do the transpose or adjoint operation. This paper did exactly that for finding the adjoint of equations (2) and (5), but the derivative and convolutional adjoint operations were readily found in Claerbout and Fomel (2014). When implementing the methods it is important to use the dot product test to make sure the adjoint operations are implemented correctly. More information on the dot product test can be found in Claerbout and Fomel (2014) and Menke (2012). The dot product test was done on each of the individual operations as well as the full $\mathbf{A}$ operation with its adjoint.

6 Results

In this section we will show the results from using the theory and methods described above to solve synthetic data sets for equation (2) and (5). We will look at how the method works when we invert with a perfect forward model, and then look at what happens when we change our forward model to be imperfect. After the synthetic data sets are demonstrated we will invert a real data set from Argentina, and use all available information to do some interpretation on the data set.

6.1 Aki-Richards

The synthetic model used for this inversion is the same as in figure 3. To generate the observed data a synthetic ricker wavelet was generated (25hz dominante frequency) from the toolset in SeismicLab by M.D.Sacchi and Signal Analysis and Imaging Group (2008). A cut off angle of 50 degree was used. Figure 5 below shows observed data before and after noise was added. A Signal to noise ratio of 3 was used for the data.

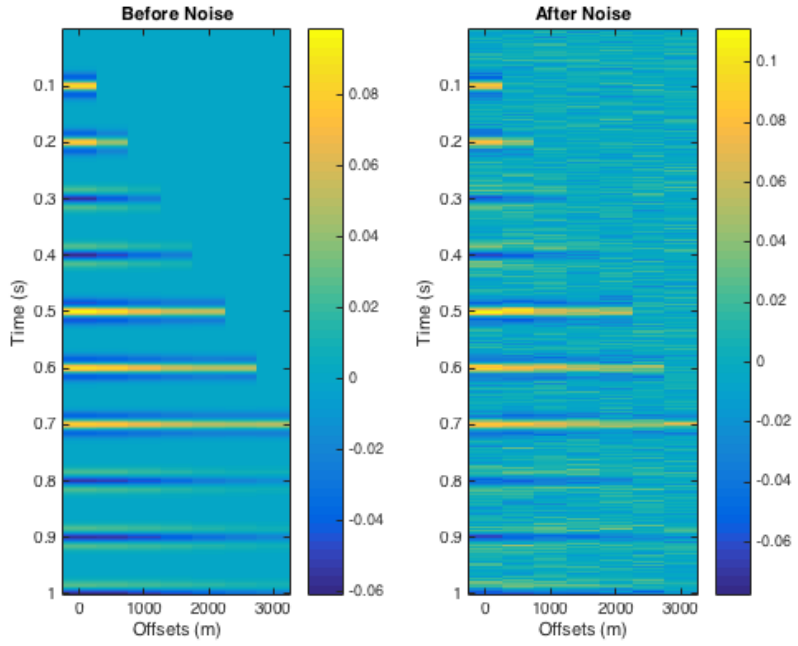

Figure 5: Observed synthetic Data for Aki-Richards equation

Using the methods as described earlier we will invert the synthetic data set using a

forward model with perfect data. Perfect means to have the same forward model as we used to generate the data. Doing this may seem like the beginning of a circular argument, but it is important for three purposes: test the inversion code, trouble shoot for bugs, and to understand the best possible case scenario. If a good result cannot be obtained for the best theoretical case no good result will be obtained and it is necessary to go back and try to refine the theory. Figure 6 shows the results of the inversion with perfect data, and figure 7 shows the data predicted from the inverse model on the left with the difference from the observed data on the right.

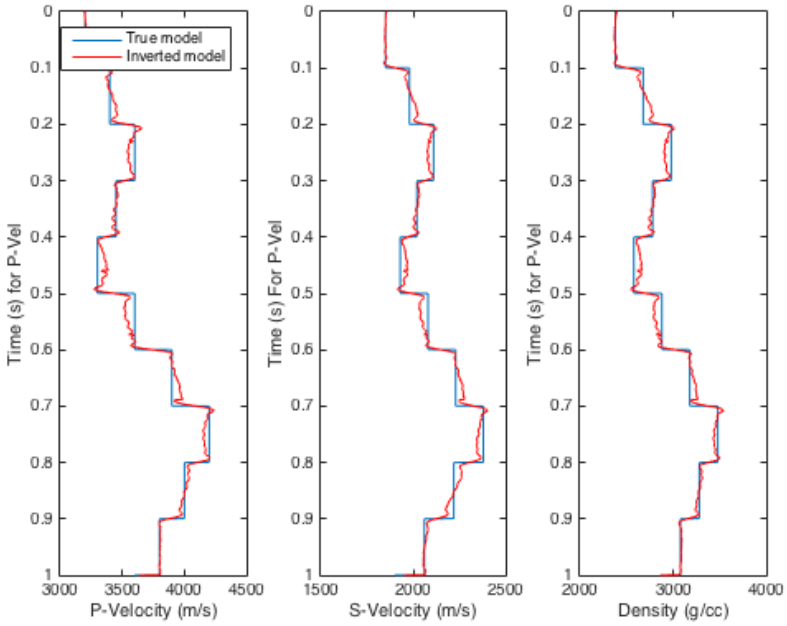

Figure 6: Inversion results using a perfect forward model.

The results look almost perfect, which is as expected. For the readers who are familiar with inverse theory, they might have made the very reasonable assumption of expecting band-limited results given our choice of norm. This issue will be discussed in the discussion section.

It is now shown that if our forward model is perfect we can get perfect results, but what happens when the forward model is not perfect. Appendix figure 22 is an example of inverting the exact same dataset but using a 15hz wavelet instead of the 25hz wavelet used to generate the synthetic dataset. The predicted data is the same as in figure 7.

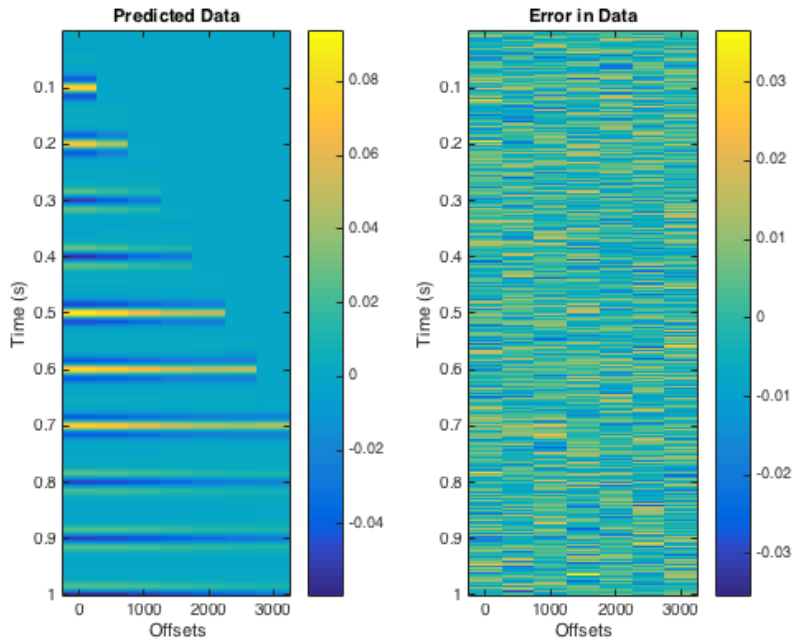

Figure 7: Predicted data using a perfect forward model.

The results are band-limited and not reasonable at all. The reason for this is the wavelet is to broad so the model has to have the huge wiggling effect to match the predicted data. Appendix figure 22 is clearly not interpretable, and it demonstrates how important it is to get a wavelet right is when tying a well. Appendix figure 23 inverts using a wavelet with a dominant frequency higher than what was used in forward modelling.

The higher frequency wavelet introduces some artificial structure, but has a predicted data identical to figure 7. Appendix figure 24 shows the background model used for the inversion, and appendix figure 25 shows the solution when the background model is not correct. This inversion was done with the same 25hz wavelet but with a background model that is fit with a fourth order polynomial instead of a 10th order polynomial for the synthetic data. The sharp changes show up well the model is shifted from the mean smooth background.

Appendix figures 24 and 25 show results that are meant to clearly outline what signatures show up in the inverted model when the forward model is incorrect. It demonstrates the importance of taking the time to get the smooth background model, and the wavelets correct to fit the data well. In this paper the real data set wavelet is estimated from

the dataset using a function called *smoothspectrum.m* in Seismic Lab mentioned above (M.D.Sacchi and Signal Analysis and Imaging Group, 2008). The next inverse model for this section is below where we used this method to estimate the wavelet from power spectrum of the synthetic data. The estimated wavelet is then used to invert the data, and appendix figure 26 shows the inversion results.

Comparing the results from our wavelet estimates it appears that the function in Seismic Lab is over estimating the dominant frequency of the wavelet. The results are still easily interpretable from the inverted model, but it again shows how much of an effect the wavelet has on the data. The next figures for this section shows what happens when we add noise to the model to make the covariance deviate from being perfect. Appendix figure 27 shows the inverted model overlaying the noisy dataset and appendix figure 28 shows the same recovered model overlain on the true model. The signal to noise ratio in the logs is about ten, and it is shown that the noise has little effect on the inversion.

The last set of figures shows what happens when we have to estimate the depth to each point to approximate the incidence angle. This was done two ways for comparison. One is using RMS of the P wave velocity from the well logs to estimate depth, and the other is using the background velocity to estimate the depth. Appendix figure 29 shows the results from using the VRMS of the P wave velocity to estimate depth, and figure 8 shows the results from the background velocity. The inversion with the VRMS velocities shows a similar patterned to inverting with the 15hz wavelet. The model gets to be quite band limited because the theta values are so out the model gets this harmonic pattern to make up for the forward model lacking. The model is still interpretable, and those large spikes can be smoothed, but when comparing to figure 8 it is quite clear what works best for this synthetic model. Another way to approximate the incidence is through ray tracing, but it was not used in this paper due to lack of access.

The results here show the inversion model is most sensitive to the wavelet and incidence. The results with a poor background model are not surprising because as shown in the theory and methods section the forward model is blind to the background model. The results show that the method is sound and needs no more regularization to produce a stable inversion.

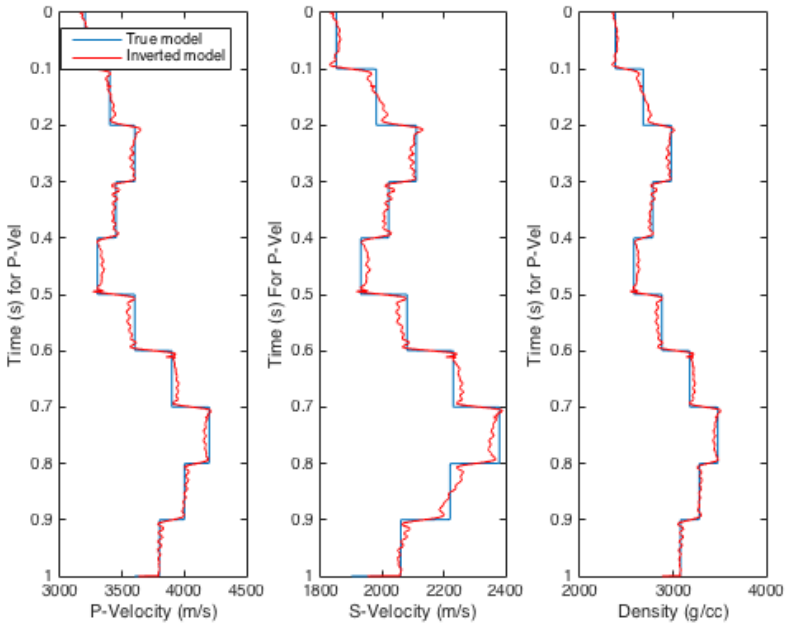

Figure 8: Inversion results using the background p wave velocity as depth.

6.2 Rüger Equation

Equation (5) accounts for the reflectivity when there are vertical fractures present. The Rüger equation shows the variation in reflectivity with azimuth relative to the strike of the vertical fractures and requires a 3D geometry. This section will demonstrate the results for a synthetic data set with variations in anisotropy with depth and show how the method works with equation (5). This section will show inversion of synthetic data for a 3D geometry with fractures varying with depth. The data set has nine azimuths, but four are shown, a 25hz minimum phase wavelet is used, the signal to noise ratio is five, and the cuttoff angle is 50 degrees. Figure 9 shows the reflection data for four of the azimuths generated, and appendix figures 30 and 31 show the initial and smooth model for the data set.

What makes this methodology convenient is the modularity. To use the Rüger equation we can use the exact same code, (if done right), and just have to change our code for equation (2) for equation (5). Since equation (5) just has the job of taking using the derivative of the parameters to generate the reflectivity, the rest of the code does not care how the reflectivity is generated, it simply takes it and does the operation, and because of this

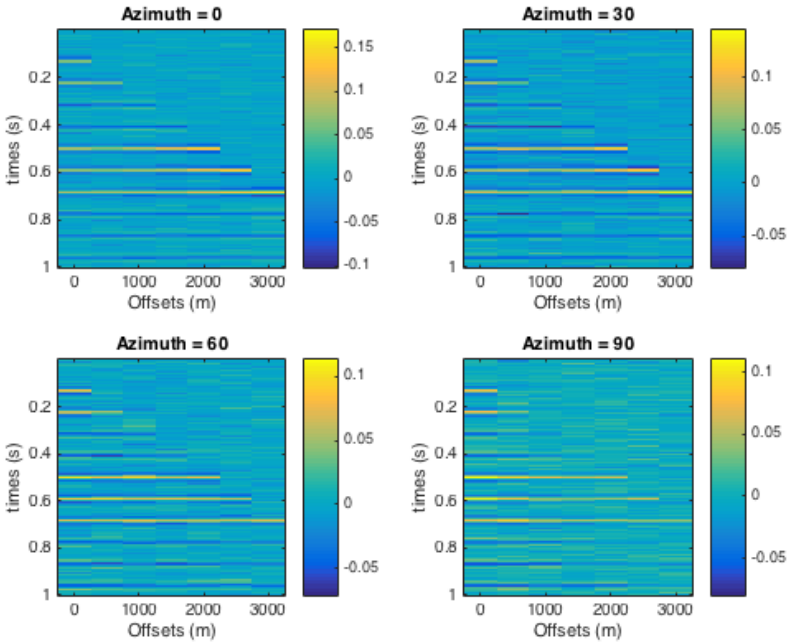

Figure 9: Synthetic data from the Rüger equation.

we can expect the results to be very similar to when we use (5). Figures 10 and 11 show the inversion results using a perfect forward model, and as expected we get nearly perfect results. The predicted data is shown in appendix figure 32.

The results with a different wavelet, and background model are the exact same as with the Aki-richards equation, the only result that may be different is the noisy ground model. Appendix figures 33 and 34 show the inverted models with noise added to the ground models. The reason for this suspicion is because equation (5) looks at the derivative of the Thomsen parameters, and not the derivative of the logarithm, so it was interesting to see how sensitive they would be to noise. However the results in appendix figures 33 and 34 show the covariance from the well logs keeps them well behaved.

The results from inverting the synthetic data for the case of vertical fractures shows to be very similar to the isotropic case, and this is quite encouraging. Unfortunately it was not possible to get real data with vertical fractures to try the inversion, but the fact the results are so similar gives a good indication that using this method for real data would be successful.

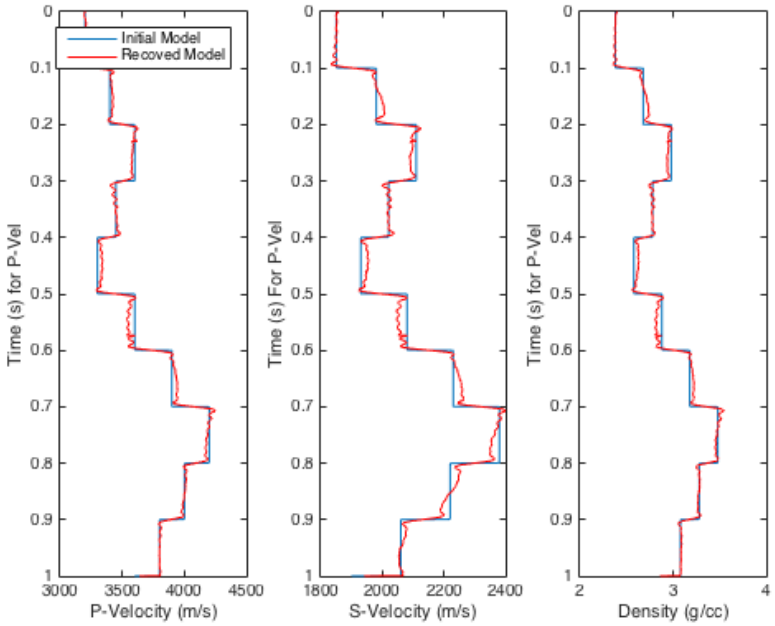

Figure 10: Inversion results of material properties using a perfect inverse model.

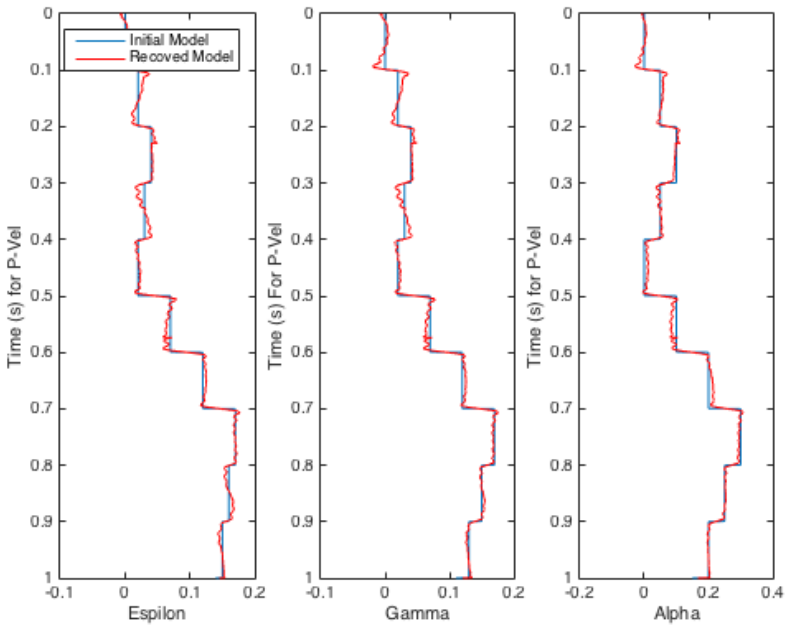

Figure 11: Inversion results of Thomsen parameters using a perfect inverse model.

6.3 Puesto Peter Field, Austral Basin, Argentina

Puesto Peter field, Austral Basin is found in the country of Argentina, which is just 150km north east of Rio Gallegos in the Santa Cruz province. The main reservoir is a marine sandstone and produces primary light oil and is on average about 1.6km deep, however there are more shallow zones ares as well (Soldo, 2009). The light oil gives a low density allowing for a high impedance contrast and giving a seismic anomaly of a standard bright spot, and is classified in Soldo (2009) as an AVO class III, which shows an increase in amplitude with wide offsets. This area a very good candidate to test our inversion scheme. The light gas and oil will give many density anomalies meaning using equation (3) is not ideal because of the low density anomalies, and using (4) means we would need to leave out the valuable offset data that will have large amplitudes past the 30 degree incidence cut off. This exact data set has been seen in Alemie and Sacchi (2011) where they use a sparse inversion to invert for the material perturbations. Data from the same field is also seen in Soldo (2009) where they invert using a stochastic simulated annealing inversion method. Figure 12 shows the stacked seismic image of the area.

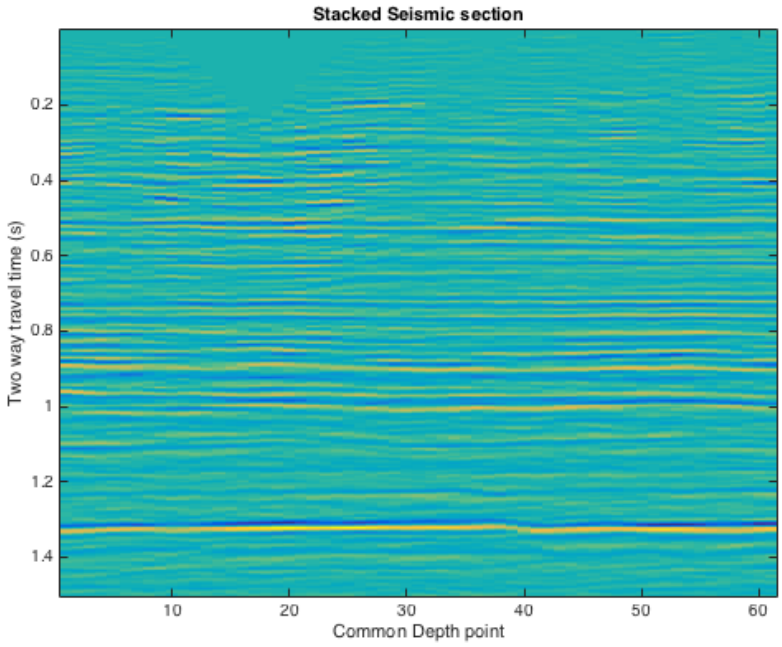

Figure 12: Stacked 2D seismic line from Puesto Peter Field

As mentioned above many brightspots can be seen in the stacked dataset, which as talked about in Soldo (2009). The amplitudes increasing with offset can be seen in on the left in figure 13. Looking closely at the reflector at around 1.3s the amplitude increasing sharply with offset. The right image in figure 13 shows the calculated incidence angles. Well data was only available from 0.5s to 1.4s in the seismic so instead of using the smooth background model to calculate incidence angles won't work since the upper 0.5 seconds are missing. The RMS of the P wave velocity from the well data was used to estimate depth and calculate the incidence angles. Figure 14 shows the provided and tied well data, with a smooth background model fit. Like in the methods section the background response was calculated to make sure it was not contributing to the seismic response. Appendix figure 35 shows the background response for our fit smooth model. Ignoring the edging effects the response is well below the noise level. This will give the smooth background model that is closest to the well logs, that does not generate a seismic response.

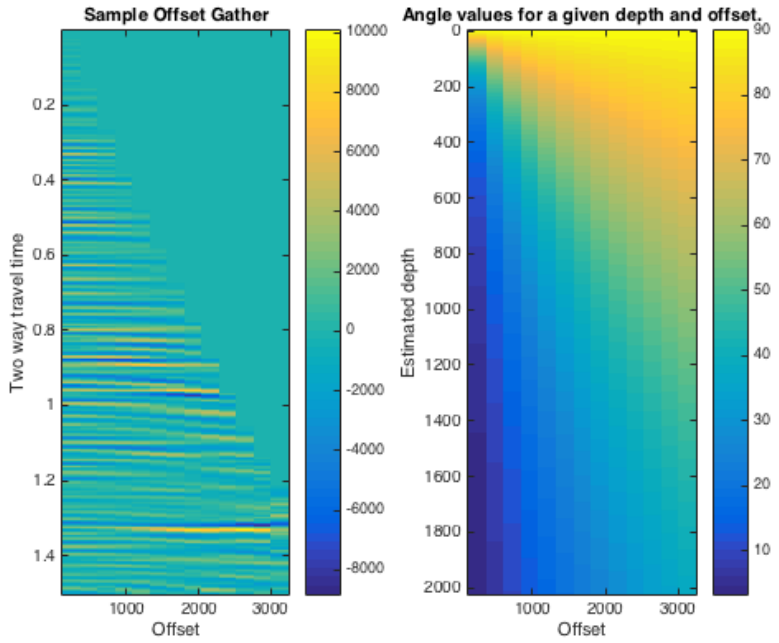

Figure 13: Sample CMP gather from Puesto Peter Field.

Before moving forward with inversion of the data there an issue that needs to be addressed in the data. Look closely at figure 13 at about 0.9s. There are events with parabolic move out in the data that are likely multiples. If we were to invert the data with these

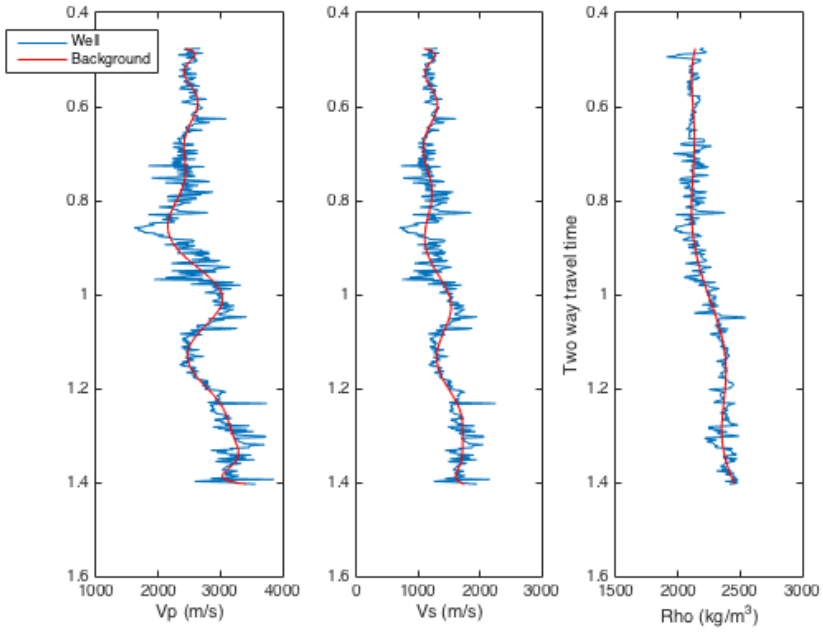

Figure 14: Well log data from Puesto field with a smooth background model fit.

moveouts they would create an artificial structure in the inverted model, which could be a costly mistake. Using Seismic Lab's parabolic movout tool from M.D.Sacchi and Signal Analysis and Imaging Group (2008) we can plot parabolic semblance to as shown in appendix figure 36. The left figure is the semblance of the CMP gather. The y axis is the time, and the x axis is the coefficient of the curvature term for a parabola. Look carefully at the intersection at about $\tau = 0.9$ and $q = 0.05$ you can see shading representing the multiple in appendix figure 36. Seismic Lab can remove this with a using sparse radon transforms to remove the multiples. For more information on how the tool works see M.D.Sacchi and Signal Analysis and Imaging Group (2008). For more information on multiple elimination see Hampson et al. (1986).

The parabolic de-multiple tool was run on all of the CMP gathers for the data set and then the traces were autocorrelated against each other to make them as flat as possible. Figure 15 shows a sample CMP at each stage of the removal. The left image is the raw CMP gather, the middle is after the multiple removal, and the right is after multiple removal and autocorrelation. The de-multiple did rather well, there are some artifacts left but it is noticeably better, and will lead to a more accurate inversion.

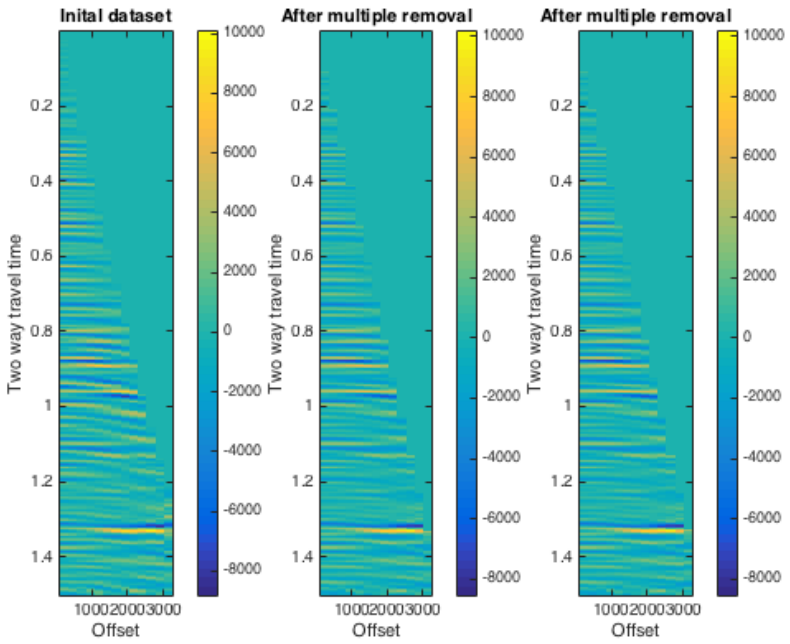

Figure 15: Images showing the effects the multiple removal. Left: before any removal. Middle: after multiple removal. Right: after multiple removal and autocorrelation.

With the multiples removed inversion can start. The amplitudes shown in the above figures are scaled down by a factor of 20,000. The wavelet was estimated as a zero phase wavelet using the smooth spectrum function from Seismic Lab (M.D.Sacchi and Signal Analysis and Imaging Group, 2008) and was calculated from the whole data set. Appendix figure 37 shows a plot of the recovered wavelet. The noise level of the seismic data was not known, so the dampening parameter (μ) was found by inverting a small set of the data, looking to see how well it fit the data, and making sure the values were similar to the values from the well logs. If the data did not fit well the dampening parameter was turned down, and if the model values were too unreasonable the dampening parameter was turned up until a good fit was reached. Once a parameter was found it was used for the entire dataset. Since each CMP is independent from one another one CMP was inverted, and then used as a starting model for the next CMP inversion. This inversion can be thought of as 61 (number of CMPs for this dataset) independent inversions, but using the previous solution as a starting point for the next solution, along with using the same dampening parameter will allow for laterally consistent results.

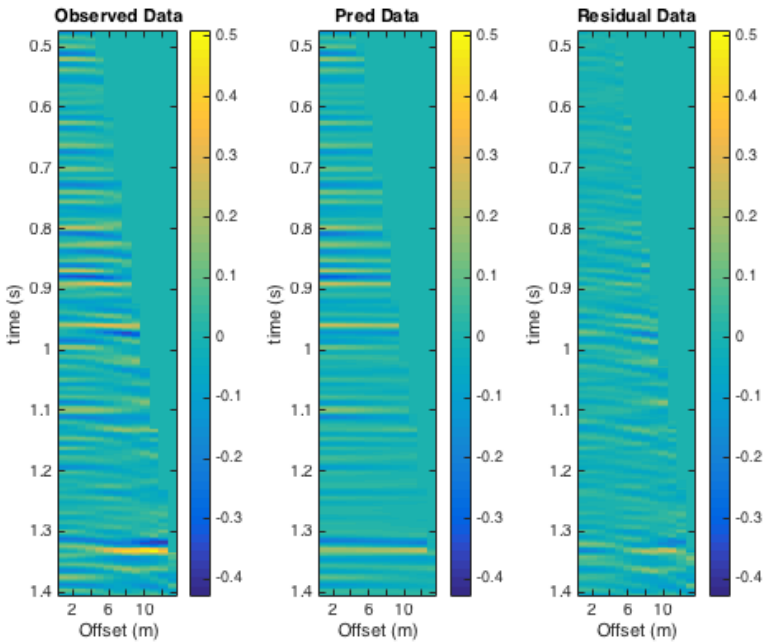

Figure 16: showing the predicted data, the predicted data, and the misfit between them for a sample CMP.

Figure 16 shows the observed data, predicted data, and misfit of the data for the CMP 1. The data fits well, but the reflection boundaries are still not completely straight, and the AVO model we have can not account for these effects. This is evident in the reflection around 1.3s. It is likely the bending in the reflection is due to some anisotropic effects or effects from horizontal layering. This can be accounted for in processing by doing to residual NMO corrections. For more information on NMO corrections and velocity analysis see Taner and Koehler (1969). Despite the one reflection at 1.3s the model appears to fit the rest of the data very nicely. Appendix figure 38 shows the inversion results from figure 16. The model looks quite good. The inverse results are quite blocky despite our choice of norm, and there are no real artifacts from the model being wrong demonstrated in the results previous section. One could argue the p wave spike around 0.95s, but everything else fits so well it is likely a real feature. The inverted section follows the well logs quite closely, and is well within the range of the well logs. With the trade off parameter found, and the sample inversion looking reasonable the next thing to do is invert the entire data set.

Inversion of the entire dataset is really fast. If care is taken to make the forward model run efficiently: the entire inversion flow can be run in under a minute for the this data set on a Macbook Pro computer. This is very convenient for experimenting with different parameters for inversion. Theune et al. (2010) implemented a scheme to try to influence lateral continuity in the model parameters, the parameter required some experimentation for their real data set. If we wanted to implement this it would be simple to find the parameter because of the low computation time. In fact any other regularization or parameter weighting can be implemented, and test pretty simply because of the modular and fast nature of the code. The inverted entire inverted data set is shown in figure 17.

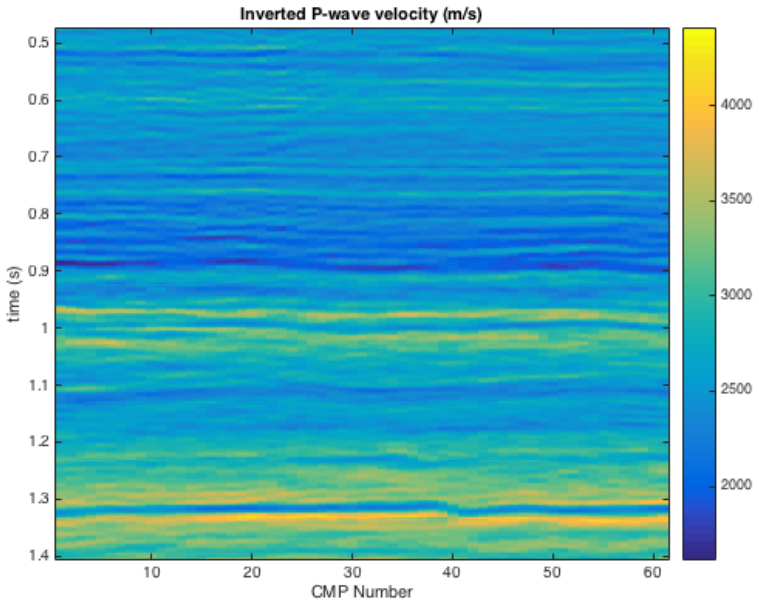

Figure 17: inverted P wave velocities from the data set.

Comparing figures 17, 18 and 19 to figure 12 we can see the results look very reasonable. The bright troughs correspond to lows in the model. The likely reservoir locations can be picked out in our inverted model. The models fall with in the values from the well logs, and shows likely geological results from looking at the seismic section. The models so good lateral continuity without having to weight solutions with lateral continuity. With seismic data of reasonable quality it is not needed to impose such conditions, because it is the seismic itself imposing the lateral continuity in the model, and trying to weight lateral

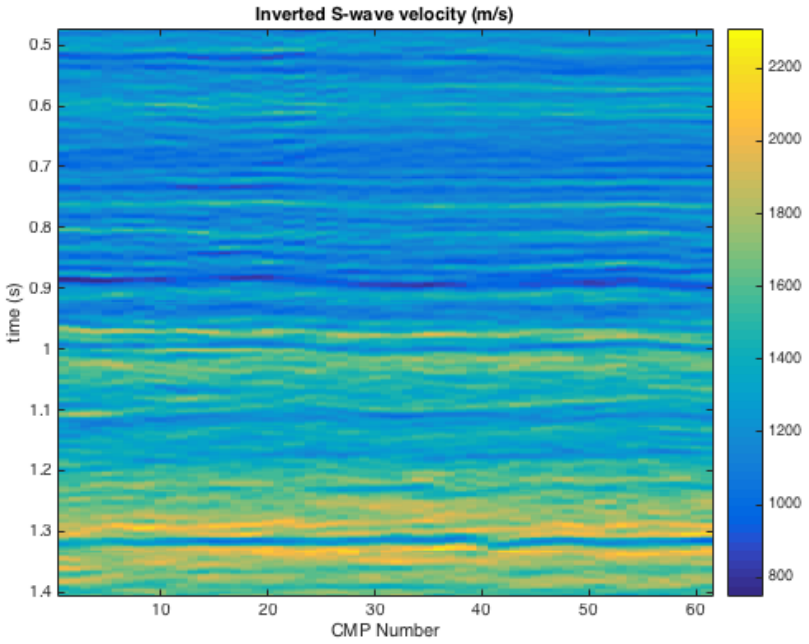

Figure 18: inverted S wave velocities from the data set.

continuity by more than the seismic will make the inversion more complicated, and could possibly introduce artifacts into the data that can led to misinterpretation.

We have successfully developed, and implemented a method for doing a pre-stack AVO/AVAz inversion that works on real data. The algorithm is fast, can use more data that most two term approximations, and the only assumptions made about the data are ones from physics, and from well log data. The method is the same for both of the forward models introduced, and is easily interchangeable for each case: the isotropic (equation 2), and the vertical fractured anisotropic (equation 5). Synthetic data was only used for equation (5) but with the synthetic results fitting so closely for each case it is likely this method will allow successful inversions on real data. The next section will go into a discussion about the results of the synthetic and real data sets.

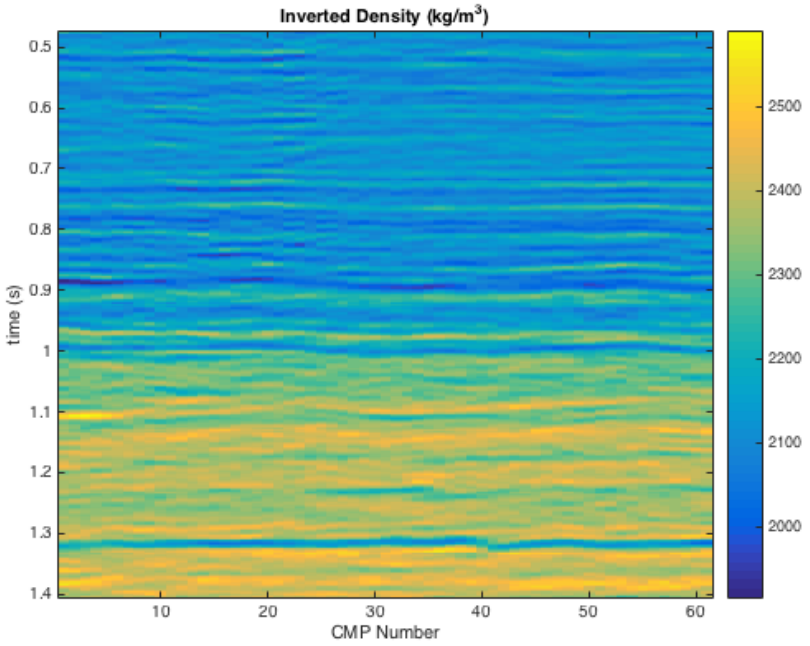

Figure 19: inverted density from the data set.

7 Discussion

7.1 Pros and cons of covariance regularization

This paper demonstrated a method using regularization to find a solution closest to the smooth background model with covariance similar to that of the well logs. The algorithm uses the physics of the problem and known data about the area to find a model that will fit the data. The other two term models introduced in this section either only use data with small incidence angles, or make an assumption about density, but it is important to see both of the methods are doing the same thing. They model the physics of the problem with assumptions.

The crutch of the method in this paper is that the well log data closely has to resembles the data in our seismic set and has to estimate a reliable covariance matrix. These assumptions are generally reasonable, but in geoscience there is always exceptions to the rule. For example if the well log data used is really far away from the area being inverted then it is less likely the properties at the well log are going to be similar to the properties in the seismic area. Using covariance in the regularization term also makes the assumption

that covariance matrix is invertible, can be decomposed with SVD, can be inverted again, and still not be ill conditioned. If this does not work the data will introduce large amounts of error into the model. It is highly recommended the covariance matrix, the regularization matrix, and the preconditioning matrix be looked at before using this method to invert, however some scripting languages like Matlab will warn you when a matrix is getting ill-conditioned. This method is not that different from the other methods, but rather just a change of assumptions and while it is likely to be good most of the time it is the job of a good geoscientist to recognize when the assumptions are flawed.

This method excels if we have good well log data because we can don't have to give up data from our assumptions, and we get behaviours similar to the a prior data from the well logs. The method also allows us to have a control over the data set. If there are unconformities where the material behaviour changes drastically that can easily be accounted for. Using equation (3) does not allow us to do that. For large data sets with multiple wells we can use location based covariance using the covariance near wells to have a great influence on the model parameters than far ones. Or the geoscientist can pick which well they want to have influence based on things locations of unconformities or faults. The method does trade simplicity for accuracy and control, and the downside is that things can go very wrong if they are used improperly, so a warning to invert with caution. This method is optimal with good well control that represents the geology of the area you are inverting.

7.2 Regularizing for blocky models

In Alemie and Sacchi (2011), Theune et al. (2010), and Downton et al. (2004) the cost functions have an extra term, or a different regularization norm that was not included in this paper. This term is to include sparsity in the derivatives of the parameters, which will give solutions which are more blocky rather than smooth. Most stratigraphy follows this bed pattern so it is very reasonable to want to get blocky models based on our a priori knowledge of the stratigraphic beds. This paper did not include the block promoting regularization term, but still had blocky results on a lot of the synthetic inversions. Even when the wavelet was wrong like in appendix figures 23 and 26 the solutions still appear to be blocky. Given

the L_2 norm promotes smoothness rather than sparsity it is a little puzzling why this is the case, but it is most likely from regularization of the covariance matrix. Appendix figure 38 even shows a lot of blocky sections. Adding in a regularization term that promotes sparsity such as L_1 makes the equation non-linear and using a method like IRLS is generally needed. IRLS was used by Alemie and Sacchi (2011) using a Cauchy distribution to solve the cost function. The trade off by using sparsity is that you will have more run time. I actually tried to implement blocky solutions from Theune et al. (2010) for this paper, but could not get a good result. Implementing blocky solutions will increased runtime, added a large amount of complexity to the problem, and as seen in this paper blocky solutions are still achievable if the covariance is relatively accurate. It would be recommended to try and implement blocky solutions if your covariance matrix is not that well defined, blocky solutions are very clear in the well logs, and you have extra time to run and tune the solution.

7.3 Inversion results from Puesto Peter Field

The available information on the regional geology of this field is minimal. At the time of writing this paper only Soldo (2009) could be found with information on this field, which is odd since Puesto Peter field is referred to as mature. The field's main reservoir is referred to as M3 layer: a marine sandstone that is said to have "very good" petrophysical qualities with a permability of 500mD and a layer thickness of about 35m (Soldo, 2009). Another reservoir of interest mentioned in Soldo (2009) is called M2 with less good petrophysical characteristics of permeabilities that are no bigger than 20mD. The tectonic setting of the basin is shown in Sachse et al. (2015) to be a foreland basin starting in the late Cretaceous. Appendix figure 40 shows stratigraphy of the section included with unconformities.

Rossello et al. (2008) looked at the petroleum geology of Tierra del Fuego Island, which includes the Austral basin. Figure 39 shows a stratigraphy with petroleum events chart for the basin and puts Puesto Peter field in the Arroyo Candelaria/ Riobueno shallow marine sandstone package right in the beginning of the Paleogene. The package is likely sealed but the overlying Dorotea Rio Turbio shales, and the source rocks are likely from the deep marine early Cretaceous pelites and mudstones. Rossello et al. (2008) states the migration

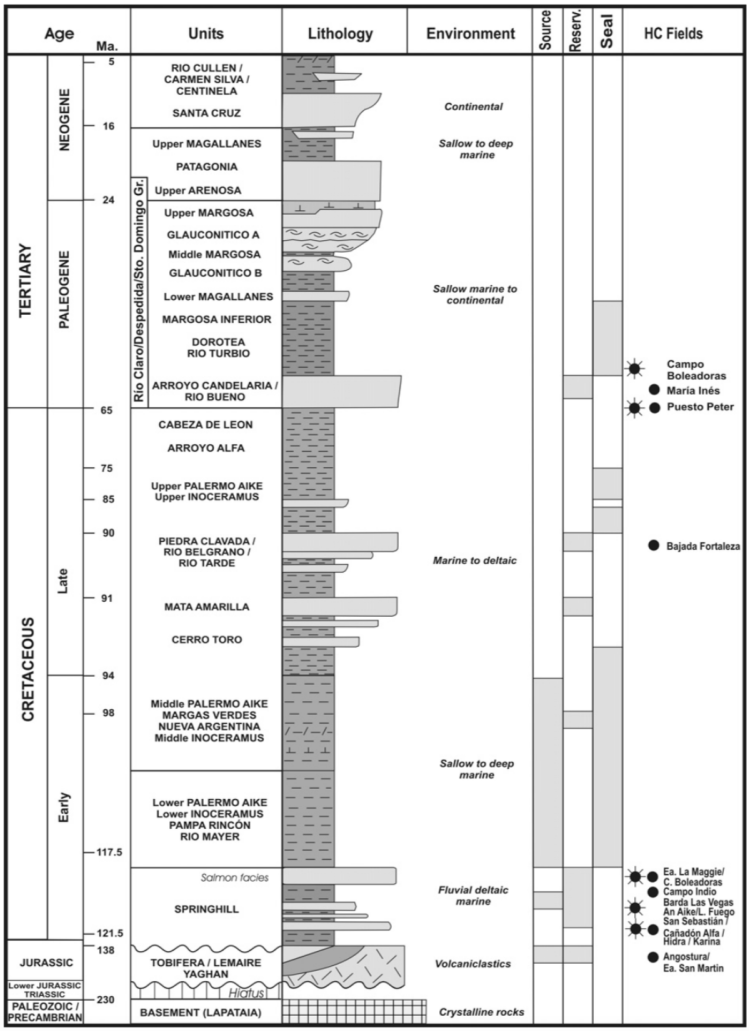

Figure 20: Stratigraphy and events chart for the Austral basin. Black stars produce gas and oil, while black circles produce oil. Figure from Rossello et al. (2008)

paths of hydrocarbons in the lower Tertiary would have migrated vertically from the Maragas Verdes unit in the early to mid Creatacous. The source rocks in the Maragas Verdes are also mentioned in Rossello et al. (2008) to have a TOC content of 1 to 2 percent, and a hydrogen index of 150 to 550 mg/g.

Getting this geological information is extremely important because we need to verify our assumptions, know what our depositional setting is for interpreting things like Vp, Vs, and rho into lithology and reservoir characterization. Appendix figure 40 shows the major unconformities in the subsurface units. While there are one or two shown above in the subsurface unit they are not carried over into the lithostratigraphy, and this gives us an ex-

cellent basis for our assumptions that the covariance generated from the well logs is a good representation of the geology. We can see the interpreted deposition environments from figure 39 and appendix figure 40 that there is a slight transgressive to regressive sequence. We can expect there will be a higher velocity and density in the deeper marine environment. Higher sea level will allow the finer, softer, shaley particles to settle out giving lower porosities which higher density and faster velocities. Interpretation of the lithology in the area would be a great deal easier with a gamma ray log, which unfortunately was not available. Comparing the information from the stratigraphy charts to our results from the inversion the trends begin to come more clear. We can see the general cyclic trends in the data from Vp, Vs, and ρ, that likely represent the rise and fall of sea level. The material properties are also sensitive to fluid saturation in pores and compaction, so it is not recommended to look too closely, but look at the general trends.

The M2 and M3 reservoirs that are mentioned in Soldo (2009) are represented by the bright trough at about 1.3s on figure 12. M2 is stated in Soldo (2009) to have a large gas cap, and that is represented by the sudden drop in density and velocities in the well logs in figure 14. This fits the inversion data as the reflector is now represented by an anomalous low in material properties that is easily interpretable given all of the above information as a reservoir. The anomalously high material properties above can be interpreted as the seal rock stopping the hydrocarbons from escaping to the surface. There are other areas with similar properties as the main reservoirs shown higher up in the inverse models as well. A promising target could easily be the reflector at about 1s, which is likely the Lower Mangallanes shown in figure 39. Lower Mangallanes is mentioned in Soldo (2009) to be a known hydrocarbon reservoir.

A common interpretation technique mentioned in both Soldo (2009) and Chopra and Castagna (2014) is to look at the Vp/Vs ratio as a gas identifier. The Vp/Vs ratio looks at the same properties Poisson's ratio. The physical reason behind using Vp/Vs is that Vp is going to drop significantly in a gas zone, compared to a zone with oil or water, but Vs will not change nearly as much in gas zones, relative to zones with water or oil. Areas with anomalously low Vp/Vs ratios are a good candidate for gas zones. This can help identify gas caps, or zones with large amounts of gas. Figure 21 is below and shows the Vp/Vs ratio

for the inverted section.

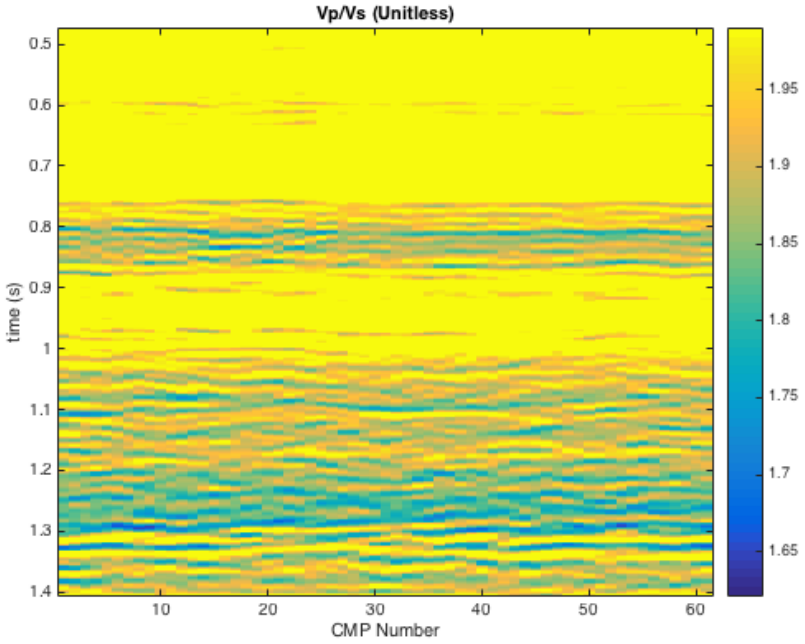

Figure 21: Vp/Vs ratio from the inverted data set. Colorbar ranges from the lowest value to the mean value.

Figure 21 has the colorbar range skewed to the minimum value to the average value of the Vp/Vs ratio to assist the eyes with interpretation. The lows are easily seen in the main reservoir at 1.3s, where gas is known. Another large anomaly is at 0.8s as well, which when looking at the original inverted figures can be easily seen, but without the help of figure 21 could have been missed. Chopra and Castagna (2014) gives a Vp/Vs range for a clean, well lithified sandstone to range between 1.6 to 1.7 and will be higher otherwise. This range also helps for the lithology discrimination given the depositional environment, and the Vp/Vs range is higher than in Chopra and Castagna (2014) but this is likely due to effect from fluids and some clays or cements. The inversion gives a good start for interpretation and is in very good agreement with what we found in the geological data.

Chopra and Castagna (2014) makes an point about seismic attributes that is relevant in this paper. It states that seismic attributes do not add any information to the data, but it just changes the way the data is looked at. I would add and say this is even true for inversion. We took all of our available data (Seismic, well logs, geological, physical) and

found a model that fit the data. Notice no extra information was added, but the data was just reformulated into something that is much easier to interpret. This, I feel, is the main reason for inversion, that is, the ease of interpretability. With the ease of interpretability highlights the importance of making sure assumptions are understood because those assumptions are built into the inverted model for interpreting, so as a rule: know your assumptions, have a basis for using those assumptions, and know the limitations your assumptions put on the inversion. If we do not adhere to these rules an error can lead to a costly misinterpretation.

8 Conclusions

This paper examined the methodology for wide angle AVO/AVAz inversion problem. The method uses well log data to help constrain the ill conditioned nature of the full linearized forward models that relate material properties to seismic traces. The paper successfully inverted and interpreted a real data set from Puesto Peter field in Argentina, using well logs, seismic data, and used geological data to bring meaning the the model that was inverted, and to make sure the inverted model made sense with what is known about the area. The results and interpretation highlighted some key areas that could be looked at to indicate the hydrocarbon potential. The data was a good choice for the AVO inversion problem because the amplitude anomalies at large offsets meant all the the data was needed for an accurate inversion, and the anomalously low densities in the reservoirs meant using Gardner's relation could introduce significant error. The results made sense with the geology and did not have any signatures of the forward model being horribly wrong shown in the synthetic models.

Synthetic models were both created and inverted to demonstrate the legitimacy of the method and to show what signatures would be left in the model when the forward models were wrong. The synthetic tests carried out showed that inversion was quite sensitive to the wavelet. For the case of data generated with a 25hz wavelet and inverting using a 15hz wavelet the model was very bandlimited and uninterpretable. The forward model also showed to have a sensitivity to the incidence angles being out when inverting, so it is recommended to use the best approximation available when needing to estimate incidence.

The smooth background model found in the well logs captures a lot of the slowly changing trends, and it is found from the well logs because seismic is blind to slowly varying trends, so when picking a background model it must generate an insignificant seismic response. It was shown that seismic itself was not enough to generate a good working model and well logs were used to find the background model and the relationship between the three, or six, material parameters. Both equations (2) and (5) were tested and found to give similar results on synthetic data.

The ambiguity and ill-conditioned nature of the AVO inversion problem was investigated, and it was found that the well logs could overcome the shortcomings and give a full, reasonable solution from using known data from the field. The method was set up using a cost function to use the forward model to fit the field data while making sure the model we were trying to find was close to the smooth background model we found from the well logs, and the materials properties had similar covariance as found from the well logs. The solution was too big to use a closed form solution, so a CGLS algorithm was used with a change of variables to generate the solution that was solved from the theoretical solution.

Forward modelling is the act of using model parameters to generate data, while inversion is using data to generate estimate model parameters. Inversion suffers from ambiguity and is often needed to be supplemented with a priori knowledge to get a reasonable solution. This paper investigated two forward models for its inversions: the Aki-Richard's equation, and the Rüger equation. The Aki-Richard's equation assumes isotropic material, while the Rüger equation assumes material with vertical fractures. The Rüger equation is very important for estimating material properties in unconventional shales and carbonate reefs that are prone to vertical fractures. The forward models used in this paper are used because they can make the least assumptions about our material property, but need to be regularized with well log data to help with the ill-conditioned nature of the problem.

AVO/AVAz are important concepts in geoscience for reservoir characterization, and using the physical models that describe their behaviour help with understanding the material properties in the reservoir. Using inversion techniques on AVO/AVAz data, combined with a priori knowledge can generate earth models that can make interpretation of data much easier that by just looking at the data itself, however the assumptions, and limitations are in

the earth model as well, so it is important to understand what assumptions are being made and to make sure the earth model is valid, or else costly mistakes will be made. AVO/AVAz inversion is a powerful tool when it is in the hands of capable geoscientists who can properly analyze the data given to them to make the best decision with the data given.

References

Aki, K., and P. Richards, 1980, Qualitative seismology: Theory and Methods.

Alemie, W., and M. D. Sacchi, 2011, High-resolution three-term avo inversion by means of a trivariate cauchy probability distribution: Geophysics, **76**, R43–R55.

Buland, A., and H. Omre, 2003, Bayesian linearized avo inversion: Geophysics, **68**, 185–198.

Chen, H., X. Yin, S. Qu, and G. Zhang, 2014, Avaz inversion for fracture weakness parameters based on the rock physics model: Journal of Geophysics and Engineering, **11**, 065007.

Chopra, S., and J. P. Castagna, 2014, Avo: Society of Exploration Geophysicists, volume **16** *of* Investigations in Geophysics.

Claerbout, J. F., and S. Fomel, 2014, Geophysical image estimation by example.

Close, D., S. Stirling, D. Cho, and F. Horn, 2010, Tight gas geophysics: Avo inversion for reservoir characterization: CSEG Recorder, **35**.

Downton, J. E., L. R. Lines, et al., 2004, Three term avo waveform inversion: Presented at the 2004 SEG Annual Meeting, Society of Exploration Geophysicists.

Gardner, G., L. Gardner, and A. Gregory, 1974, Formation velocity and density-the diagnostic basics for stratigraphic traps: Geophysics, **39**, 770–780.

Gidlow, P., and G. C. Smith, 2003, The fluid factor angle: Presented at the 65th EAGE Conference & Exhibition.

Goodway, B., J. Varsek, and C. Abaco, 2006a, Practical applications of p-wave avo for unconventional gas resource plays: Part, **1**, 16.

———, 2006b, Practical applications of p-wave avo for unconventional gas resource plays: Part, **2**, 52–65.

Hampson, D., et al., 1986, Inverse velocity stacking for multiple elimination: Presented at the 1986 SEG Annual Meeting, Society of Exploration Geophysicists.

Lines, L., 1999, Avo and density: Canadian journal of exploration geophysics.

Mahmoudian, F., G. F. Margrave, and C. Joe Wong, 2012, Avaz inversion for anisotropy parameters of a fractured medium: Technical report, Tech. rep.

M.D.Sacchi, and Signal Analysis and Imaging Group, 2008, Seismic lab.

Menke, W., 2012, Geophysical data analysis: discrete inverse theory: Academic press.

Nafe, J. E., 1957, Reflection and transmission coefficients at a solid-solid interface of high velocity contrast: Bulletin of the Seismological Society of America, **47**, 205–219.

Prioul, R., A. Donald, R. Koepsell, Z. E. Marzouki, and T. Bratton, 2007, Forward modeling of fracture-induced sonic anisotropy using a combination of borehole image and sonic logs: Geophysics, **72**, E135–E147.

Rossello, E. A., C. E. Haring, G. Cardinali, F. Suárez, G. A. Laffitte, and V. A. Nevistic, 2008, Hydrocarbons and petroleum geology of tierra del fuego, argentina: Geologica Acta, **6**, 55–67.

Roxana Varga, T. H., and J. Pendrel, 2013, How to maximize recoverable reserves in an unconventional reservoir using reservoir characterization from 3d seismic: a barnett shale case study: CSEG Recorder, 64–70.

Rüger, A., 1997, P-wave reflection coefficients for transversely isotropic models with vertical and horizontal axis of symmetry: Geophysics, **62**, 713–722.

Sachse, V., F. Strozyk, Z. Anka, J. Rodriguez, and R. Primio, 2015, The tectonostratigraphic evolution of the austral basin and adjacent areas against the background of andean tectonics, southern argentina, south america: Basin Research.

Scales, J. A., 1987, Tomographic inversion via the conjugate gradient method: Geophysics, **52**, 179–185.

Sil, S., 2013, Fracture parameter estimation from well-log data: Geophysics, **78**, D129–D134.

Smith, G., and P. Gidlow, 1987, Weighted stacking for rock property estimation and detection of gas: Geophysical Prospecting, **35**, 993–1014.

Soldo, J., 2009, Fluid to lithology discrimination approach using simultaneous avo inver-

sion: Puesto peter field, austral basin, argentina: The Leading Edge, **28**, 698–701.

Taner, M. T., and F. Koehler, 1969, Velocity spectra-digital computer derivation applications of velocity functions: Geophysics, **34**, 859–881.

Theune, U., I. Ø. Jensås, and J. Eidsvik, 2010, Analysis of prior models for a blocky inversion of seismic ava data: Geophysics, **75**, C25–C35.

Yilmaz, Ö., 1990, Seismic data processing: Society of Exploration Geophysicists.

9 Appendix

This appendix contains figures that are referred to in the main body of the paper, but are not essential to understand the content being discussed in the main body of the paper.

9.1 Aki-Richards figures

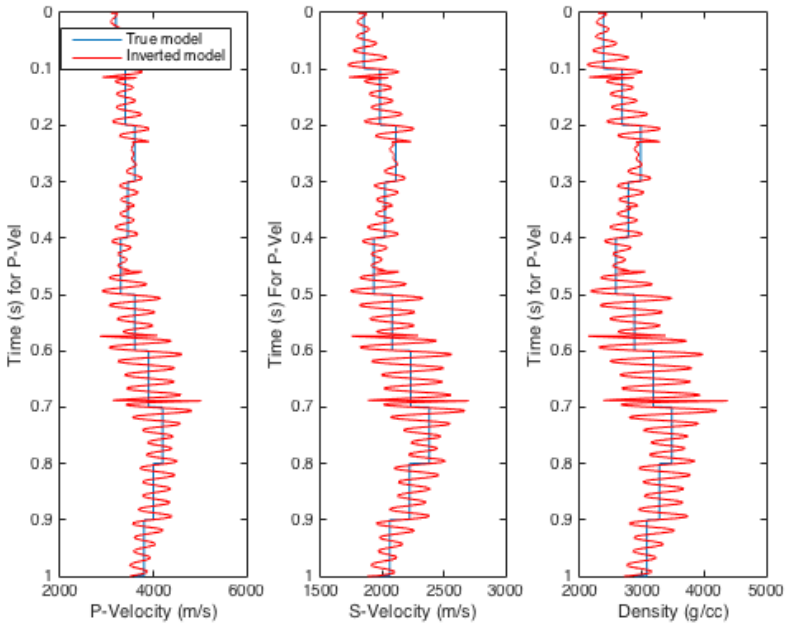

Figure 22: Inversion results using a 15hz wavelet.

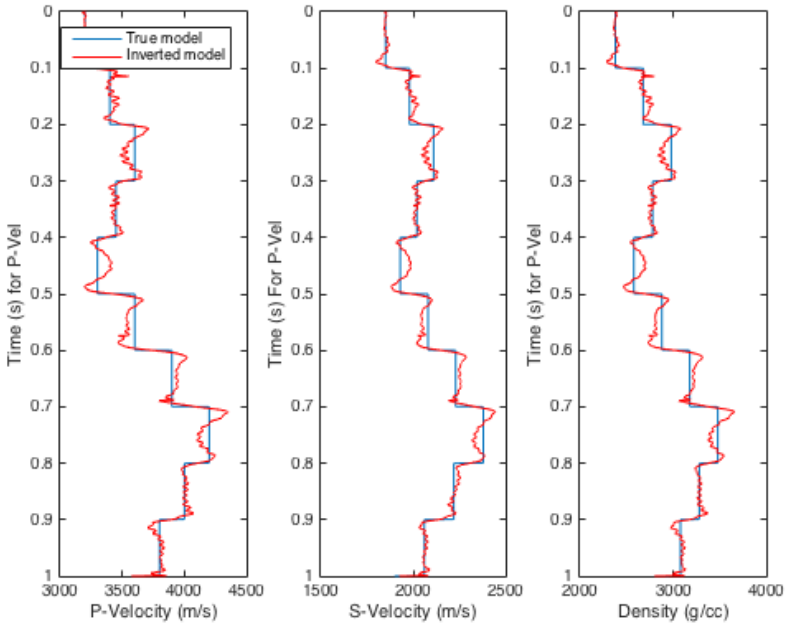

Figure 23: Inversion results using a 35hz wavelet.

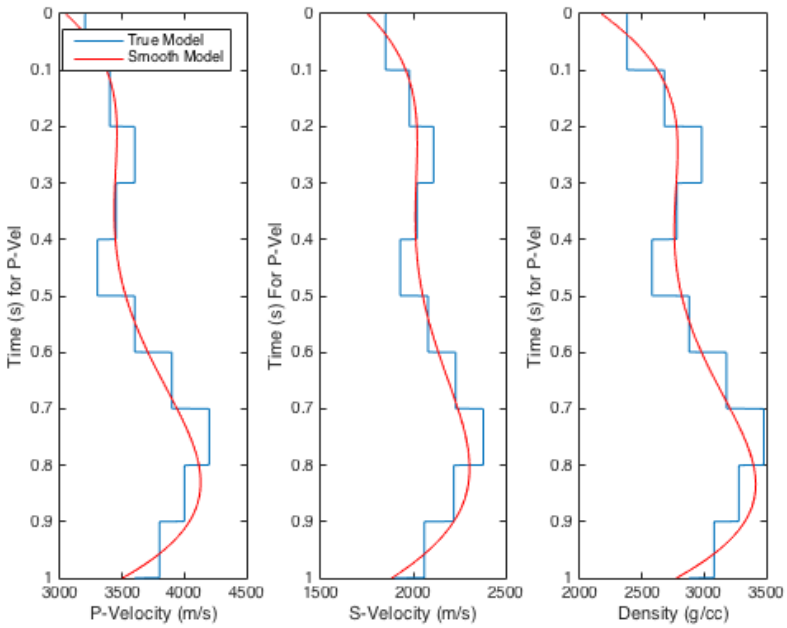

Figure 24: Fourth order polynomial background model

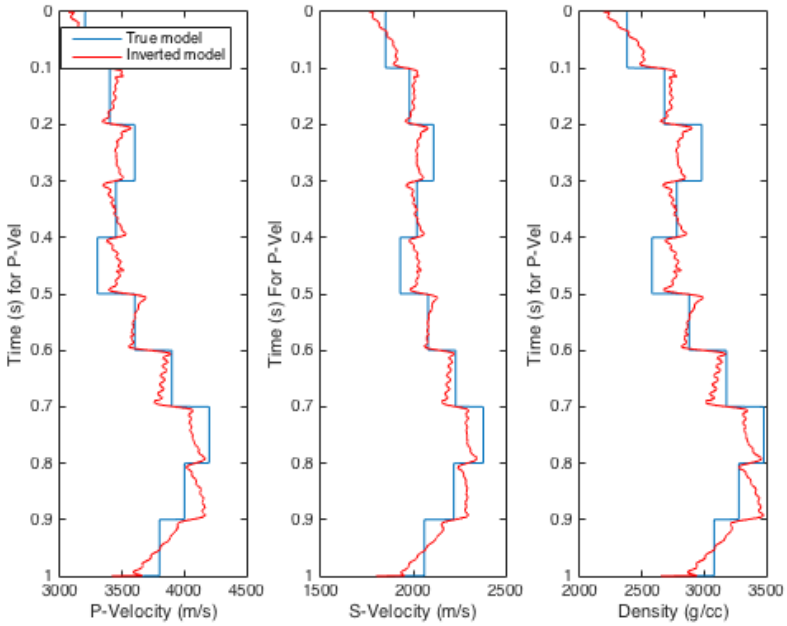

Figure 25: Inversion results using the wrong background model.

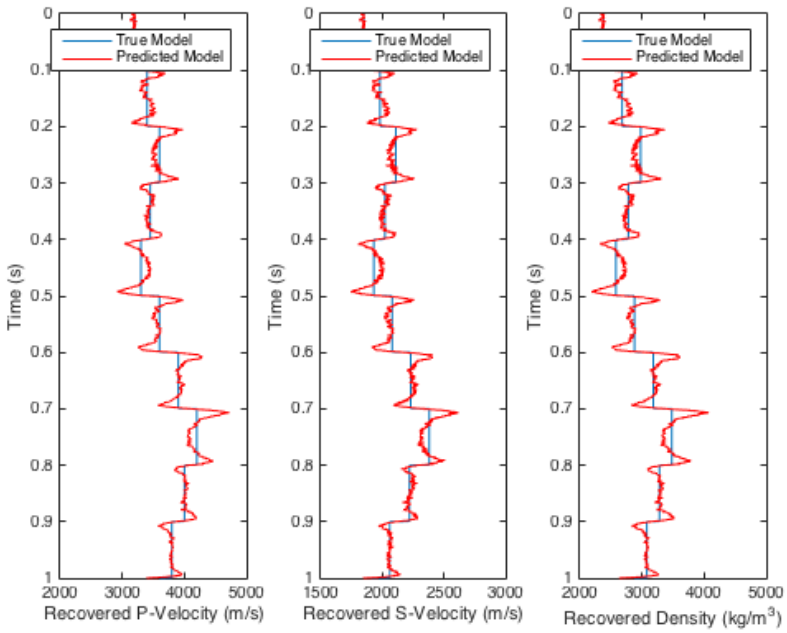

Figure 26: Inversion results using smooth spectrum wavelet estimated with SeismicLab.

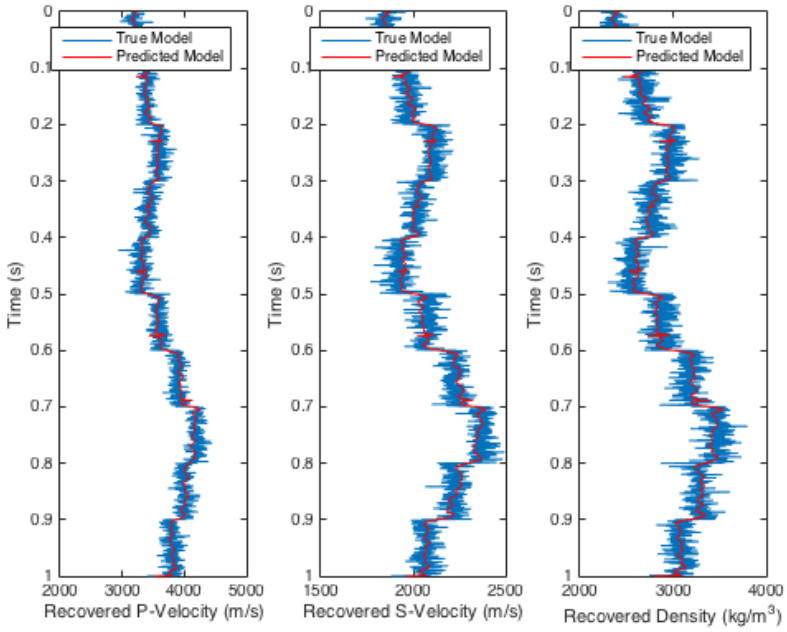

Figure 27: Inversion results for noisy well log.

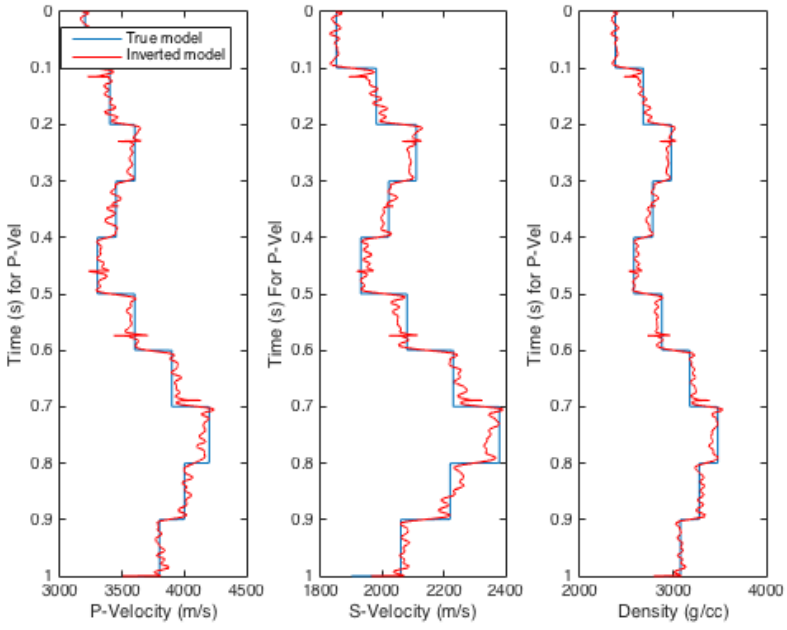

Figure 28: Inversion results for noisy well log over top the idea well log.

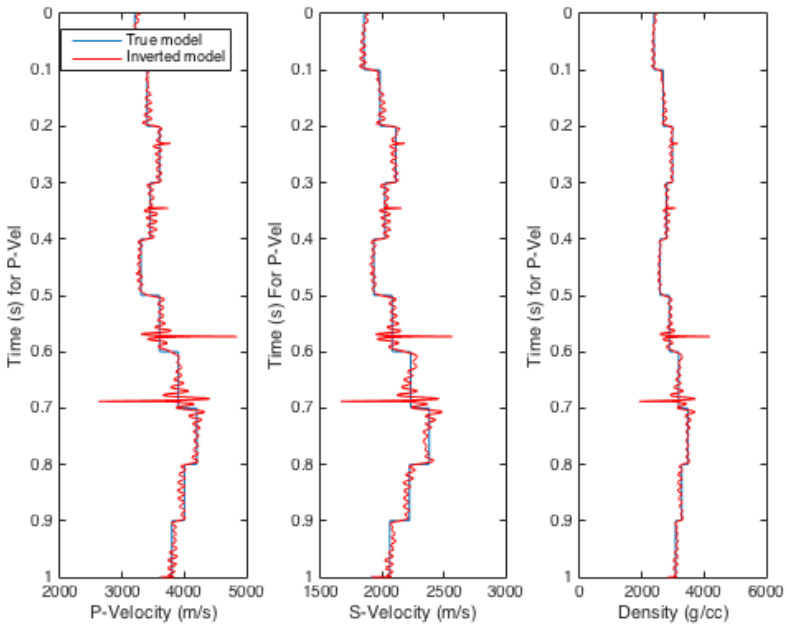

Figure 29: Inversion results using the RMS p-wave velocity to estimate depth.

9.2 Rüger Equation figures

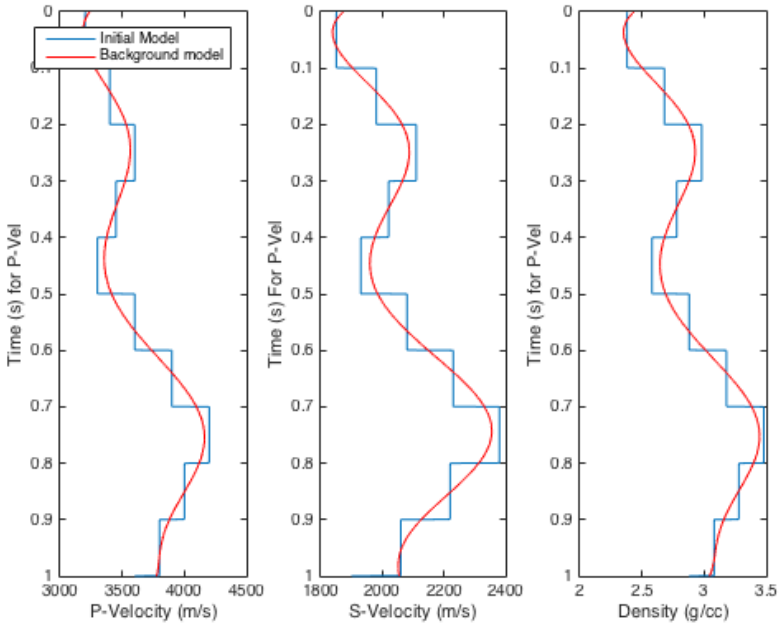

Figure 30: Synthetic model parameters for Rüger equation.

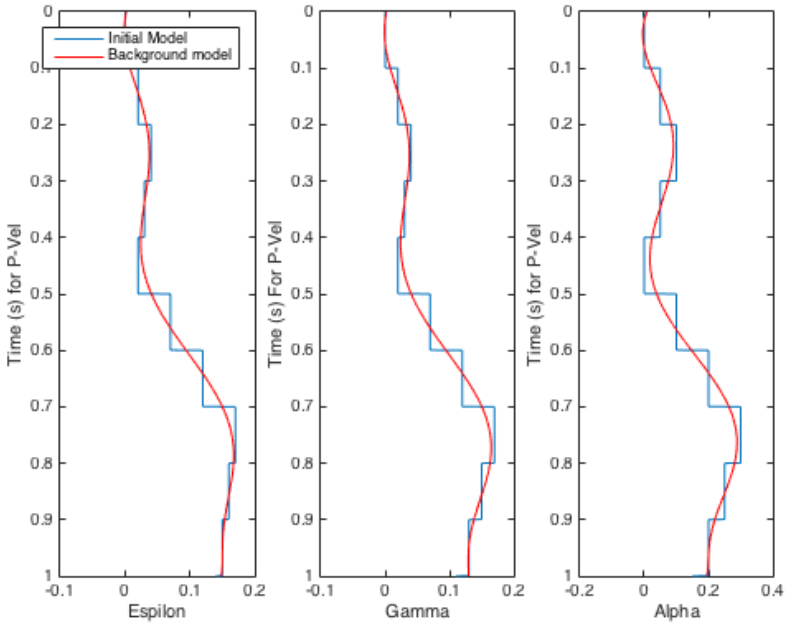

Figure 31: Synthetic model parameters for Rüger equation.

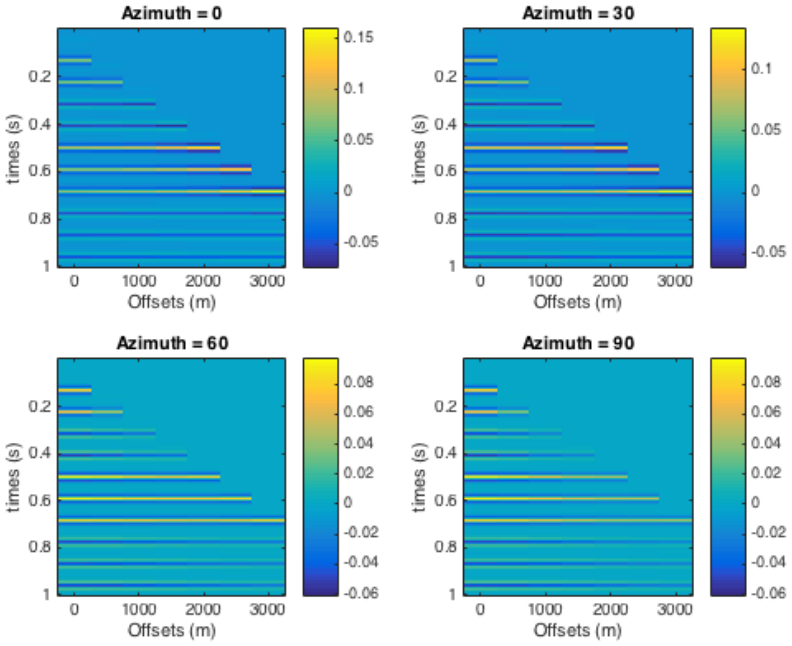

Figure 32: Predicted data using a perfect inverse model.

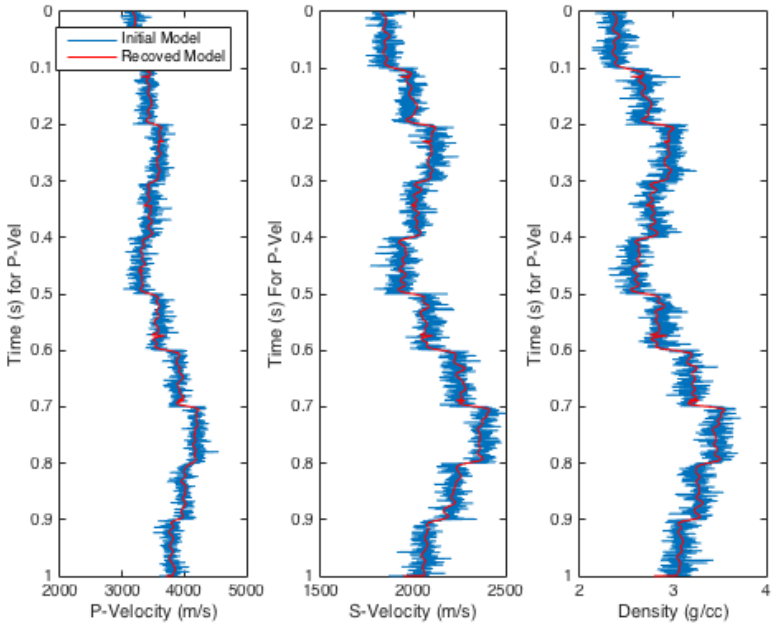

Figure 33: Inversion results of material properties with a noisy ground model.

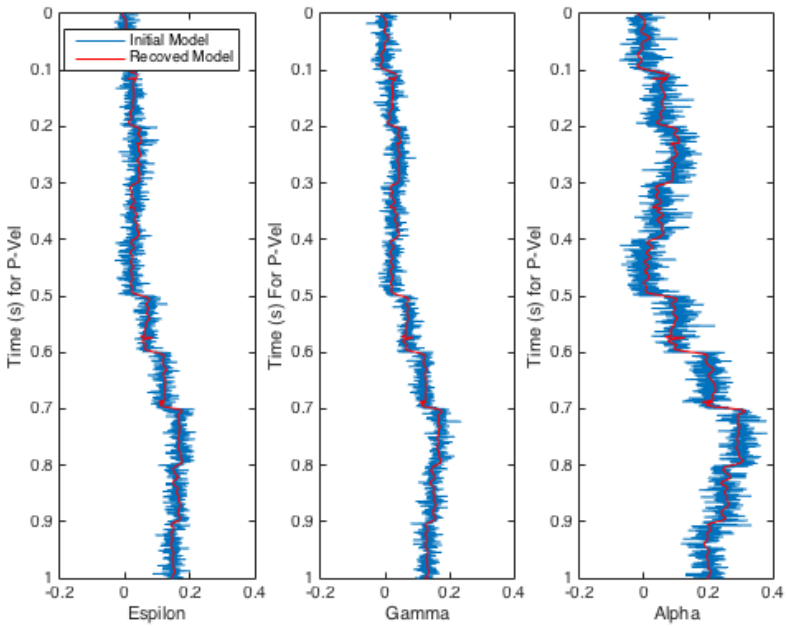

Figure 34: Inversion results of Thomsen parameters with a noisy ground model.

9.3 Puesto Peter Field figures

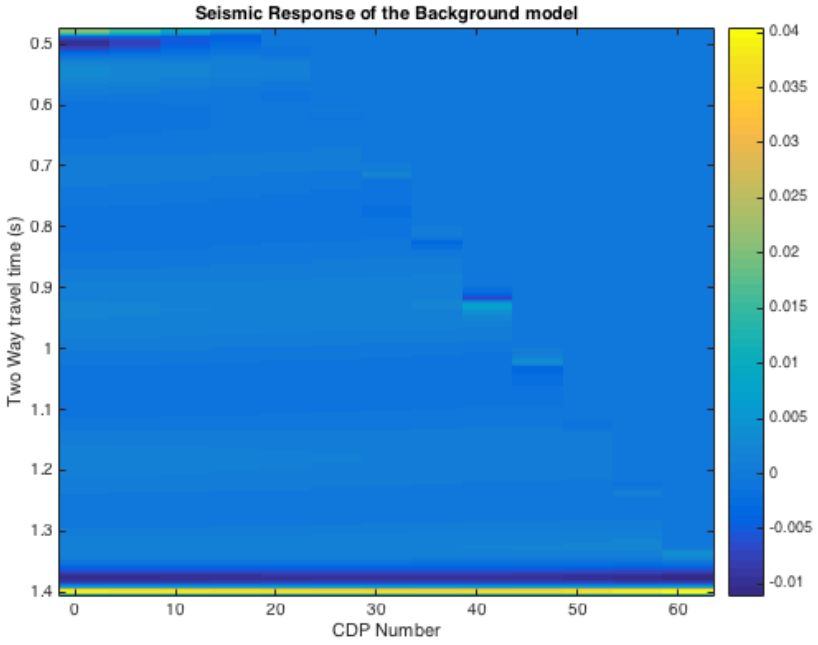

Figure 35: Calculated background model AVO response.

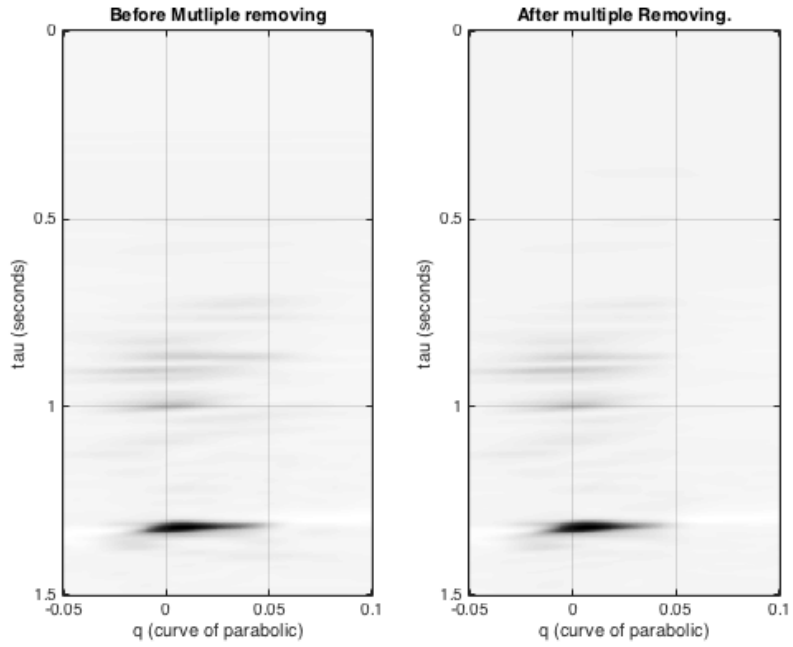

Figure 36: Parabolic semblence plot of a CMP gather.

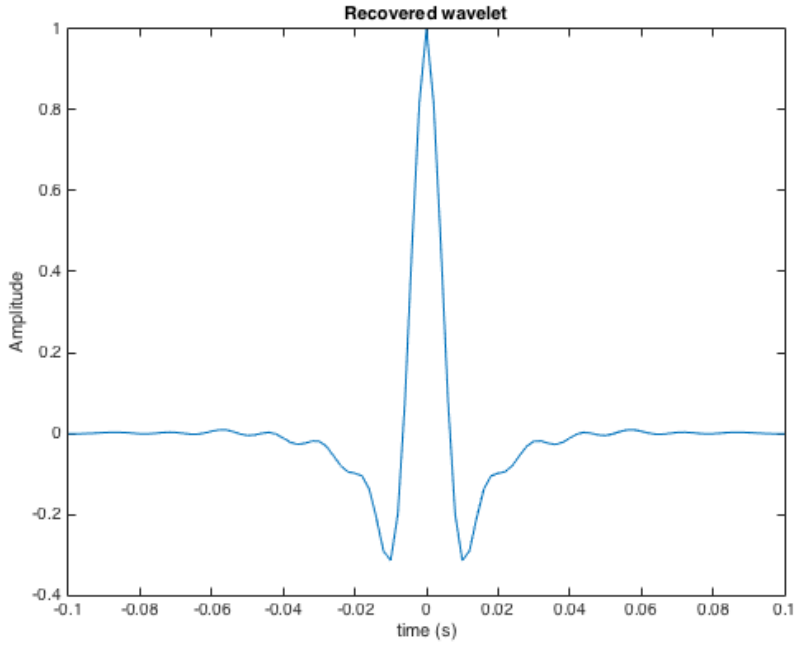

Figure 37: Recovered wavelet from the CMP data set.

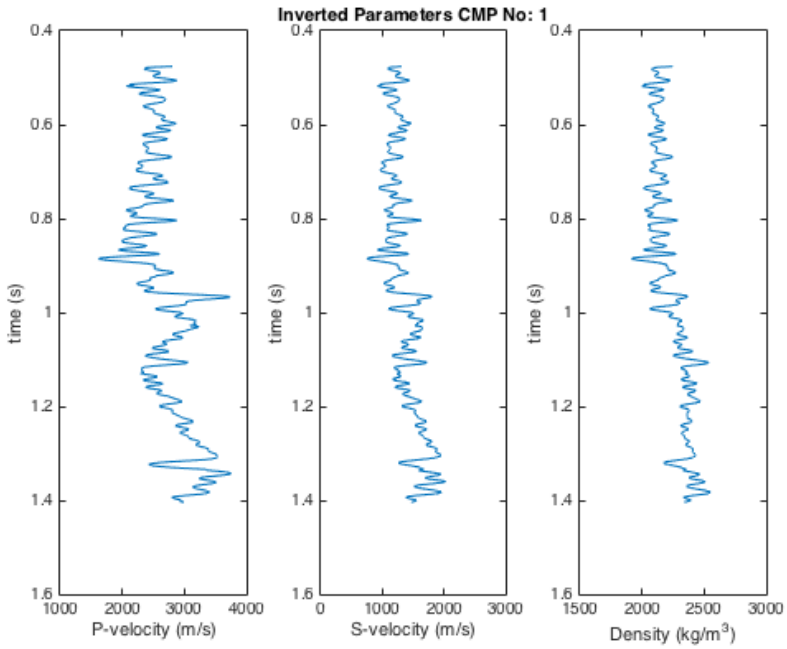

Figure 38: the resulting inversion results from inverting the sample CMP.

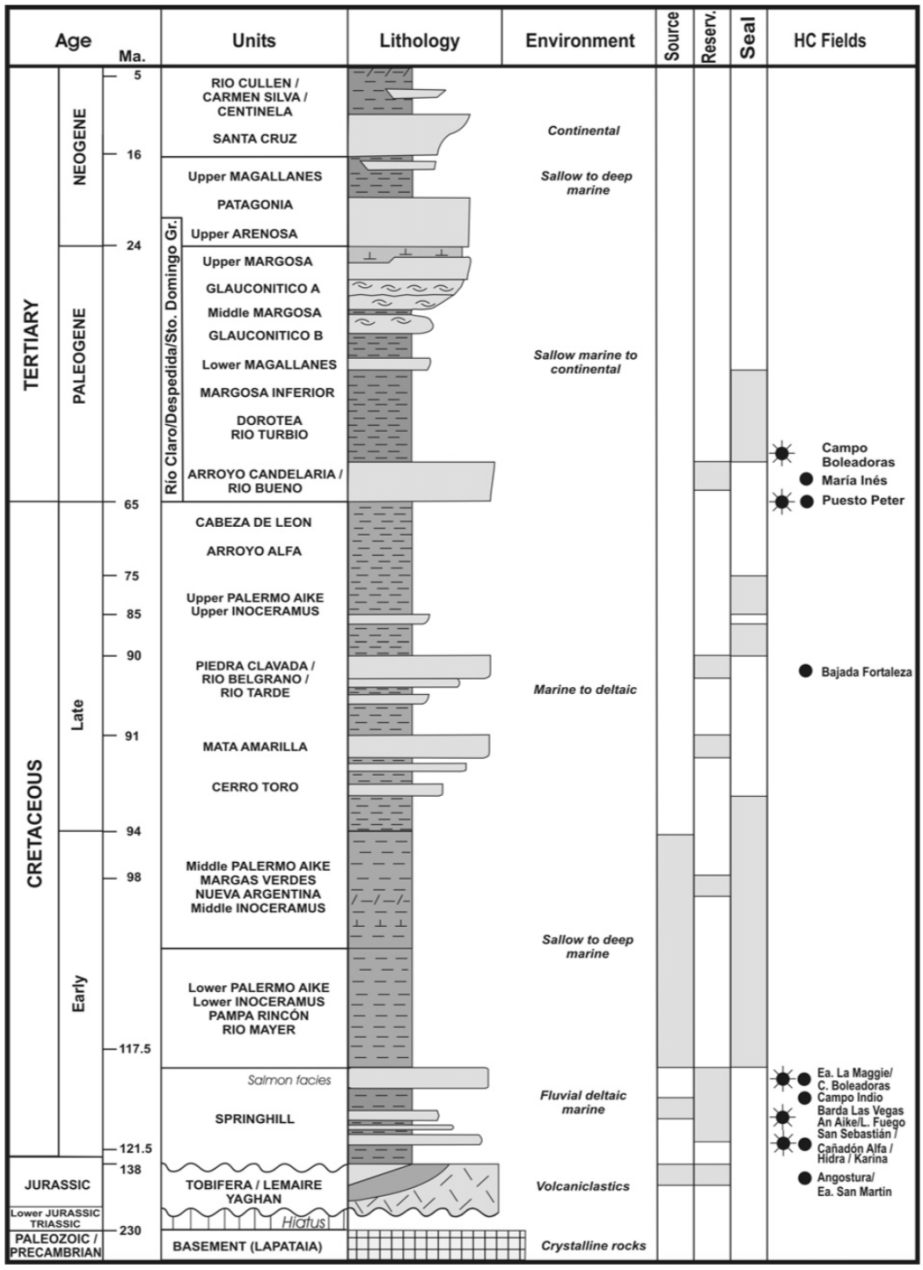

Figure 39: Stratigraphy and events chart for the Austral basin. Black stars produce gas and oil, while black circles produce oil. Figure from Rossello et al. (2008)

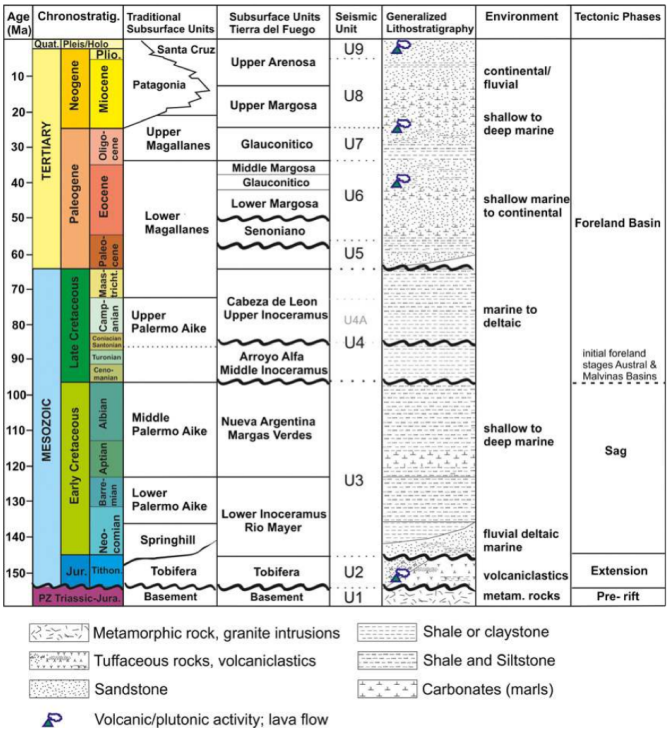

Figure 40: Stratigraphy and tectonic chart for the Austral basin. Figure from Sachse et al. (2015).